

# COHERENT NONLINEAR SPECTROSCOPY: From Femtosecond Dynamics to Control

---

Marcos Dantus

*Department of Chemistry and Center for Fundamental Materials Research, Michigan State University, East Lansing, Michigan 48824; e-mail: dantus@msu.edu*

**Key Words** ultrafast, four-wave mixing, photon echo, transient-grating, wavepacket

■ **Abstract** This review focuses on the study of the dynamics of isolated molecules and their control using coherent nonlinear spectroscopic methods. Emphasis is placed on topics such as bound-to-free excitation and the study of concerted elimination reactions, free-to-bound excitation and the study of bimolecular reactions, and bound-to-bound excitation and the study of intramolecular rovibrational dynamics and coherence relaxation. For each case the detailed time-resolved information reveals possible strategies to control the outcome. Experimental results are shown for each of the reactions discussed. The methods discussed include pump-probe and four-wave mixing processes such as transient grating and photon echo spectroscopy. Off-resonance transient-grating experiments are shown to be ideal for the study of ground state dynamics, molecular structure, and the molecular response to strong field excitation.

## INTRODUCTION

The early calculations carried out by Hirschfelder & Eyring on the dynamics of the  $H + H_2$  reaction in the 1930s revealed the femtosecond time scale of fundamental chemical processes such as bond breakage and bond formation (1). Scientists have been pushing the technological edge to be able to reach the time scale at which these chemical events occur. In the mid-1950s the resolution was in the microsecond time scale with the pump-probe work of Porter (2, 3). The invention of the laser in the 1960s facilitated the rapid progress to the nanosecond and then to the picosecond time scale (4). By 1984, scientists had arrived at the femtosecond time scale with measurements of fundamental processes such as the photochemistry of bacteriorhodopsin and the intramolecular relaxation time of large organic molecules in the gas phase and in solution (5-10). In 1985, Zewail began to probe the ultrafast dynamics of isolated molecules with subpicosecond time resolution (11), and by 1987, published the first time-resolved observation of transition states in a chemical reaction (12). The significance of these measurements, recognized by the Nobel prize in 1999, was that Zewail had captured the essence of a

chemical reaction in a system that had a well-defined reaction coordinate and was not complicated by the solvent response.

Given that the generation of ultrafast pulses has outpaced the development of ultrafast detectors, the study of ultrafast chemical dynamics requires the use of methods that involve multiple laser pulses. One or more pulses initiate the chemical reaction and one or more probe its progress. The involvement of multiple laser pulses implies that these measurements belong to the realm of nonlinear optical spectroscopy. This distinction is of importance when seeking a thorough understanding of the signals. In linear spectroscopy, one is concerned with absorption or emission. In nonlinear optics, the processes involve the coherent interaction between the sample and one or more of the laser pulses (13–15). Coherent nonlinear spectroscopic methods provide the means to study molecular dynamics and to explore laser control of chemical reactivity.

The goal for active laser control is to devise electromagnetic fields that drive the outcome of a chemical reaction in the desired direction (16–20). There are two main approaches to this problem. The frequency-resolved scheme (also known as coherent control), proposed by Brumer & Shapiro (21, 22) utilizes quantum interference between different pathways to a final state to exert control over the outcome. One of the most striking demonstrations of this scheme is found in the work of Gordon and co-workers, controlling autoionization versus predissociation in HI and DI molecules (23, 24). The time-resolved scheme (also known as pump-dump), proposed by Tannor et al (25, 26), exploits the time-dependent motion of wave packets created by ultrafast (usually femtosecond) laser pulses to manipulate the outcome of the reaction. Experimental demonstrations of this control scheme are found in many pump-probe time-resolved experiments, for example, the excitation of I<sub>2</sub> to produce either the D (<sup>1</sup>Σ<sub>u</sub><sup>+</sup>) or the F (<sup>3</sup>Π<sub>u</sub>) states (27), or the production of Na<sup>+</sup> or Na<sup>2+</sup> as a function of time delay between pump and probe pulses (28–30) and the isotopic separation of bromine (31), and more recently, the preparation of groundstate wave packets of K<sub>2</sub> (32). Wilson and coworkers generalized this approach to obtain a formalism that is more amenable for the study of thermal ensembles of molecules (33, 34).

The search for an optimal electromagnetic field in terms of spectral and temporal composition to control the outcome of a chemical reaction was formalized by Rabitz and coworkers (35, 36). Optimization of the Tannor-Rice pump-dump scheme for controlling the selectivity of product formation was considered by Kosloff et al (37). The application of chirped pulses to shape nuclear wave packets and enhance vibrational coherence was proposed by Ruhman & Kosloff (38). Broers et al demonstrated the use of chirped pulses to enhance the population transfer in the three-state ladder of the rubidium atom (39). Experimental (40) and theoretical (41, 42) studies on the effect of chirped pulses on the multiphoton excitation of molecules showed that the traditional saturation limits can be exceeded, thereby facilitating population inversion. The groups of Shank, Wilson, Leone, and others have shown experimental evidence that tailored femtosecond pulses can be

used to modify the initial wave packet formed by the excitation laser (43–53). In some cases, tailored pulses (chirp) can be used to enhance single and multi-photon transitions (54–57) as well as excitation of high vibrational states (58, 59). Experimental demonstration of optical control using shaped laser pulses on multi-dimensional systems has been shown by Gerber's group, who optimized the yield of different product channels (60). Bucksbaum's group showed selective Raman excitation of the symmetric and antisymmetric OH stretch in liquid methanol (61).

In the following sections we focus on the application of coherent nonlinear spectroscopic techniques to study isolated chemical reactions and their control, in which all laser interactions take place on a time scale that is short compared with the coherence relaxation. The protocol we follow is first to understand the ultrafast dynamics involved, selecting systems with a well-defined reaction coordinate, and then to consider a rational method for their control using lasers. We explore bound-free concerted elimination reactions and free-bound bimolecular reactions, both of which are best studied in the gas phase, in which there is no solvent cage to dictate the progress of the reaction. The section on bound-bound molecular transitions focuses on inter- and intramolecular dynamics and relaxation. Experiments using four-wave mixing methods reveal mechanisms for controlling the dynamics and energy flow. We have attempted to illustrate each section with a number of experimental results from our group, rather than attempt a comprehensive review of each topic.

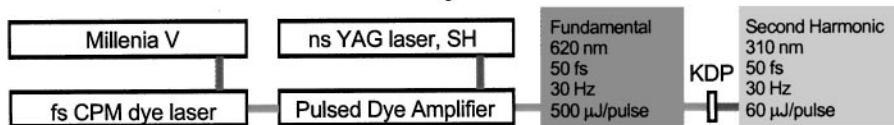
## METHODS

Advances in ultrafast laser technology have permitted the development of commercial units capable of carrying out most ultrafast experiments. For this reason, we do not describe these laser systems in detail. Instead we concentrate on describing the setups typically used for nonlinear optical measurements. The experiments described here were carried out with two types of laser systems (see Figure 1). The first is based on a home-built colliding pulse mode-locked laser (62–64) amplified by a four-stage dye amplifier (65). After amplification the system produces pulses centered at 620 nm with 0.5 mJ in energy at a repetition rate of 30 Hz. The second system is based on a Kapteyn-Murnane oscillator capable of producing 13 fs pulses when compressed. This laser is regeneratively amplified by an Evolution X pumped Spitfire (Spectra Physics). The output, centered at 810 nm consists of pulses with 0.8 mJ in energy at a repetition rate of 1 kHz. Both laser systems produce transform-limited pulses of 50-fs duration, as measured by frequency-resolved optical gating (66).

The two techniques used most frequently in our laboratory are pump-probe and degenerate four-wave mixing (FWM). For pump-probe measurements the laser, after the compression, is split into two arms of a Mach-Zhender interferometer. Typically, one beam is frequency doubled. The two pulses are then recombined and

## Experimental Methods

### Laser System I



### Laser System II

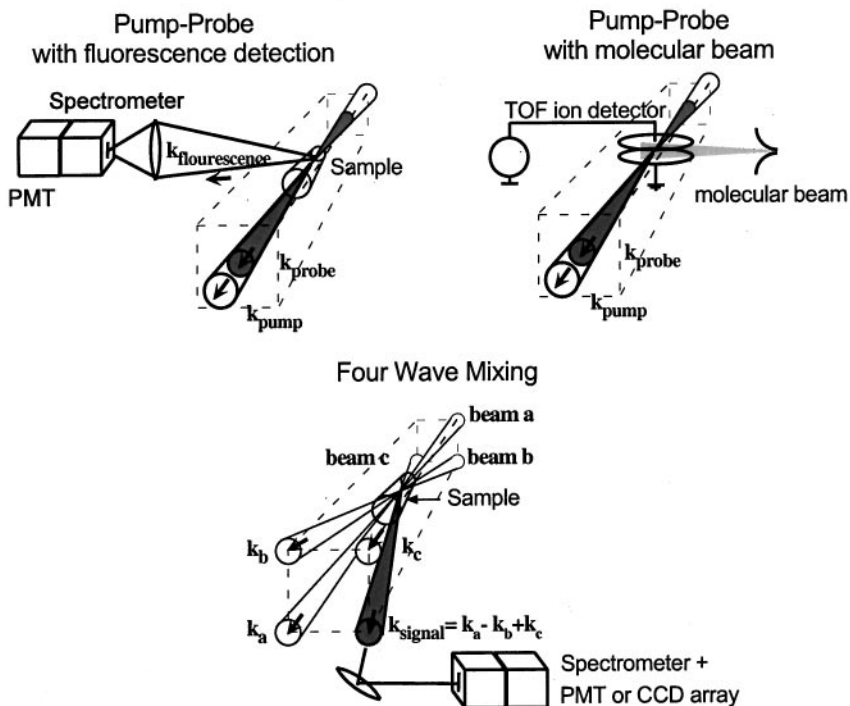
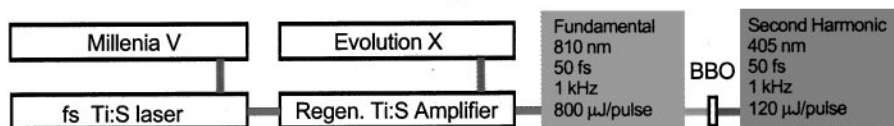


**Figure 1** (Top) Schematic of two experimental set-ups used in our laboratory with their main characteristics. (Bottom) Three most commonly used nonlinear optical techniques in time resolved spectroscopy.

focused into the sample cell and fluorescence is detected at right angles (67). When required, tunability is achieved with two-stage noncollinear optical parametric amplifier system, generating tunable  $\sim 20$ -fs pulses in the 450- to 1600-nm range (68). Gas-phase measurements can be carried out in gas bulbs or in molecular beams. The signal detected can be laser-induced fluorescence, mass selected ions, or photoelectrons.

For FWM measurements, the laser beam is split by two successive beam splitters into three beams of approximately equal intensity and attenuated down to  $\sim 20 \mu\text{J}$  each. Pulses are delayed with respect to each other by a computer-controlled actuator. The three beams are combined in a specific phase-matching geometry (69, 70) and focused by a 0.5 m lens in a quartz cell containing the gas-phase sample (see Figure 1). In this configuration the FWM signals are detected in the direction  $\mathbf{k}_S = \mathbf{k}_a - \mathbf{k}_b + \mathbf{k}_c$ . The subindices a, b, and c are used to identify the beams in space, but the pulses can take any time order 1, 2, or 3; therefore, for the same phase-matching geometry, different phenomena such as stimulated photon echo, virtual echo, transient grating (TG), and reverse TG (RTG) can be detected (71). The signal can be time integrated (homodyned) or time gated (heterodyned); similarly, the signal can be spectrally integrated or spectrally dispersed (71–75).

## BOUND-FREE TRANSITIONS: CONCERTED-ELIMINATION CHEMICAL REACTIONS

Concerted chemical and biochemical processes have been of great interest, particularly since the publication of Woodward & Hoffmann's work on pericyclic reactions (76). A concerted reaction is defined as one for which multiple fundamental changes (such as bond formation, charge transfer, etc) occur in a single kinetic step (76–79). In practice, this means that a reaction is considered to be concerted if there is no evidence of intermediate stages. Therefore, the classification depends on the sensitivity of the chosen method to detect the short-lived intermediates. A reaction that is rapid compared with the detection method could be erroneously considered concerted. Molecular beam techniques have been used to determine gas-phase reaction mechanisms (80). These methods have a temporal resolution comparable with the rotational period of the molecules ( $\approx 10^{-12}$  s) and have been useful in determining the concertedness of chemical reactions by analysis of the velocity and angular distribution of the products (81–83).

The use of femtosecond transition state spectroscopy to detect the presence of reaction intermediates was introduced by Zewail and coworkers (84). Their time-resolved experiments on the  $\alpha$ -cleavage reaction of acetone and on the decarbonylation of cyclopentanone have shown that both reactions proceed by a stepwise (nonconcerted) mechanism (85, 86). In the condensed phase, the solvent provides a "cage" that keeps the reagents and products of a chemical reaction in close proximity, making it difficult to determine if a reaction proceeds by a concerted mechanism. This determination, therefore, is ideally carried out on

isolated molecules. One example that has received a great deal of attention recently is the tautomerization reaction of 7-aza-indole (87–90). Time-resolved gas-phase measurements indicate that the two hydrogen bonds are traded in a nonconcerted fashion (87, 88).

Recently, several groups have addressed the ultrafast dynamics involved in the concerted elimination of halogen molecules following the high-energy excitation of halogenated alkanes (91–104). The reaction channel  $\text{CH}_2\text{I}_2 \rightarrow \text{CH}_2 + \text{I}_2(\text{D}')$  was first investigated by Style (105, 106) and Okabe (107). Our group has investigated the femtosecond time scale dynamics of this reaction (95, 97, 98). Huber and coworkers have studied the high-energy dissociation pathways of  $\text{CF}_2\text{I}_2$  with excitation between 248 and 351 nm. Their findings indicate that production of I and  $\text{I}^*$  constitute the major dissociation channels for the reaction at these wavelengths (83, 91, 101, 102). As in diiodomethane, difluorodiiodomethane also produces  $\text{I}_2$  following high-energy excitation; in this case, the reaction is initiated with absorption of two photons of 267 nm (101). This study did not identify the electronic state of the molecular halogen or its vibrational or rotational energetics. Schwartz et al have studied the photodissociation dynamics of  $\text{CH}_2\text{I}_2$  with femtosecond lasers in different solvents (92). Their work focused on the reaction pathway initiated by the 310-nm pump that leads to the production of  $\text{CH}_2\text{I} + \text{I}$ . They followed the geminate recombination reforming the parent molecule by measuring transient absorption at 620 nm. The initial dynamics that take place upon excitation of  $\text{CH}_2\text{I}_2$  have been studied by Duschek et al in the gas phase (108) and in solution by Kwok & Phillips using resonance Raman scattering between 342 and 369 nm (93, 94), and by Sundström and coworkers using pump-probe spectroscopy (103). Their findings indicate the involvement of the I-C-I symmetric stretch, antisymmetric stretch, and bending vibrational modes.

Femtosecond pump-probe measurements from our group showed that high-energy excitation produces molecular iodine by a concerted process (56, 95–100). Coherent vibrational motion in the  $\text{I}_2$  product was observed (95, 98, 100). Analysis of the transition state dynamics shows that the two-carbon halogen bonds are broken and the new interhalogen bond is formed within 50 fs. When the dissociation dynamics of  $\text{CH}_2\text{I}_2$  and  $\text{CH}_3(\text{CH}_2)_2\text{CHI}_2$  were compared, the transition state lifetime for  $\text{CH}_3(\text{CH}_2)_2\text{CHI}_2$  was found to be approximately two times longer than the lifetime of  $\text{CH}_2\text{I}_2$  (97, 98). Analysis indicated that the difference in lifetime could be attributed to the change in the reduced mass of the carbene fragment, therefore, the reaction occurs faster than intramolecular vibrational relaxation (IVR) to the alkane chain.

Figure 2a depicts a cut of the potential energy surfaces for this system. The pathways that lead to the production of I and  $\text{I}^*$  by stepwise photodissociation processes are shown on the left. The pathways shown on the right-hand side of the figure lead to dihalogen molecules produced through concerted elimination mechanisms, the  $\text{CH}_2 + \text{I}_2(\text{D}')$  channel, and a less probable channel leading to  $\text{CH}_2 + \text{I}_2(\text{f})$  (98, 100). The former showed very small differences for time delay

greater than zero when probed with parallel or perpendicular polarized light while the latter showed very clear rotational anisotropy (99, 100) (see Figure 2*b* and 2*c*). This rotational component of the data allowed us to have a much clearer picture of the mechanism involved in this dissociation process. Analysis of the rotational anisotropy indicated that  $I_2(f)$  is produced with a very hot rotational distribution (100). Using classical mechanical modeling of the dynamics, we confirmed that the symmetry of the molecule must be broken in the dissociation to achieve such a hot rotational distribution. An asynchronous concerted process does not conserve the  $C_{2v}$  symmetry and is consistent with the observed dynamics. A synchronous concerted mechanism in which the  $C_{2v}$  symmetry of the parent is conserved would produce rotationally cold products. In conclusion, the  $I_2(D')$  pathway is consistent with a synchronous concerted mechanism, whereas the  $I_2(f)$  pathway is consistent with an asynchronous concerted mechanism.

The concerted reaction occurs following 12 eV excitation. Electronic structure calculations are not capable of providing an accurate potential energy surface for molecules containing two heavy atoms at these high energies. In the absence of a potential energy surface, we assume, as a first-order approximation, that the parent molecule behaves as a pseudodiatom, breaking into the carbene radical and the halogen molecule, and that the fragments reach terminal velocity immediately following the dissociation. We have studied the concerted elimination of halogen molecules from a family of compounds,  $CX_2YZ$  (where  $X = H, F, \text{or}$

**TABLE 1** Energetics and dynamics for concerted molecular elimination<sup>a</sup>

Reaction	Reaction enthalpy (eV)	Energy available <sup>a</sup> (eV)	Reduced mass <sup>b</sup> (a.m.u.)	Experimental time (fs)	$E_{\text{kin}}/E_{\text{avail}}^c$
$CH_2I_2 \rightarrow CH_2 + I_2(D')$	8.38	3.62	13.3	$47 \pm 3$	0.34
$CH_2 + I_2(f)$	9.20	2.80	13.3	—	
$CD_2I_2 \rightarrow CD_2 + I_2(D')$	8.38	3.62	15.1	$47 \pm 3$	0.50
$BuI_2 \rightarrow Bu: + I_2(D')$	8.38	3.62	46.0	$87 \pm 5$	0.35
$CH_2Br_2 \rightarrow CH_2 + Br_2(D')$	10.50	1.50	12.9	$59 \pm 1$	0.52
$CF_2Br_2 \rightarrow CF_2 + Br_2(D')$	8.50	3.50	38.1	—	
$CCl_2Br_2 \rightarrow CCl_2 + Br_2(D')$	8.80	3.20	54.6	$81 \pm 4$	0.54
$CH_2ICl \rightarrow CH_2 + ICl(D')$	8.40	3.60	12.9	$48 \pm 1$	0.32
$CH_2 + ICl(G)$	9.20	2.80	12.9	$71 \pm 4$	0.19

<sup>a</sup>(95–100, 104).

<sup>b</sup>Energy available is calculated by subtracting the reaction enthalpy from the photon energy (12 eV).

<sup>c</sup>Reduced mass is calculated assuming a two-body, carbene-halogen, molecular dissociation. The lifetimes are the results of femtosecond time-resolved measurements from our group (95–100, 104).

<sup>d</sup>Kinetic energy is calculated from the experimental dissociation time (see text), and the ratio between the kinetic energy and the available energy can be used to compare energy partitioning among the different reactions.

Cl and Y, Z = Cl, Br, or I) (see Table 1). We have assumed that the potentials are similar within this family, which allows us to compare the transition state lifetimes among these compounds. If we consider that the time it takes the product to achieve terminal velocity is negligible, we can use the expression for the kinetic energy,  $E_{\text{kin}} = (1/2)\mu v^2$ , and substitute the velocity  $v$  by  $L/\tau_{\text{exp}}$ . Where  $L$  is the distance required for bond breaking,  $\tau_{\text{exp}}$  is the experimental dissociation time (i.e. transition state lifetime) and  $\mu$  is the reduced mass calculated for the pseudodiatom (carbene-dihalogen) molecule. The kinetic energy  $E_{\text{kin}}$  represents the energy available for recoil after the enthalpy of reaction and internal energy (vibrational and rotational energy) of the products have been subtracted from the photon energy.

Based on this model we can compare the dissociation dynamics of nine related concerted elimination reactions. Table 1 compares the transition state lifetimes of  $\text{CH}_2\text{I}_2$ ,  $\text{CD}_2\text{I}_2$ ,  $\text{CH}_3(\text{CH}_2)_2\text{CHI}_2$ ,  $\text{CH}_2\text{Br}_2$ ,  $\text{CF}_2\text{Br}_2$ ,  $\text{CCl}_2\text{Br}_2$ , and  $\text{CH}_2\text{ICl}$ . The data were collected consecutively, with the laser intensity kept constant to avoid apparent differences in dissociation times resulting from saturation of the transitions. For this comparison, we take the total photon energy and subtract the reaction enthalpy to yield the available energy for the reaction,  $E_{\text{avail}} = h\nu - \Delta H$ . The ratio  $E_{\text{kin}}/E_{\text{avail}}$ , where  $E_{\text{kin}}$  is estimated from  $\tau_{\text{exp}}$  as discussed above, gives us a parameter to compare the energy partitioning in the reactions and is given in the sixth column of Table 1. When  $E_{\text{kin}}/E_{\text{avail}} = 0.34$ , the energy partitioning is similar to the reaction for  $\text{CH}_2\text{I}_2$ . When the ratio is greater, more energy is partitioned into translation. Finally, when the ratio is smaller, the fragments acquire more internal energy in the form of vibrations and rotations.

The data in Table 1 can be used to estimate dissociation times. The ratio of the dissociation time is given by

$$\frac{\tau_1}{\tau_2} = \left[ \frac{(E_{\text{photon}} - \Delta H_2)\mu_1}{(E_{\text{photon}} - \Delta H_1)\mu_2} \right]^{1/2}, \quad 1.$$

where we assume that  $L_1 \approx L_2$  and  $E_{\text{kin}} \approx E_{\text{avail}}$  as a first approximation. We first compare the dissociation times of reactions with equal reaction enthalpy, such as  $\text{CH}_2\text{I}_2$  (reagent 1) and  $\text{CH}_3(\text{CH}_2)_2\text{CHI}_2$  (reagent 2), producing  $\text{I}_2(\text{D}')$ . The ratio between the experimentally determined dissociation times is  $\tau_2/\tau_1 = 1.85$  (see Table 1); the ratio of the estimated dissociation times based on Equation 1 is  $\tau_2/\tau_1 = 1.85$ . The agreement in this case is remarkable, indicating that the assumptions  $L_1 \approx L_2$  and a similar kinetic energy partition are valid. Second, we compare the experimental dissociation times of reactions having different enthalpy, such as  $\text{CH}_2\text{Br}_2$  (reagent 1) and  $\text{CCl}_2\text{Br}_2$  (reagent 2). The ratio of the experimental dissociation times is  $\tau_2/\tau_1 = 0.73$ , where the ratio of the estimated times using Equation 1 is  $\tau_2/\tau_1 = 0.71$ . The small difference between the experimental ratio and the value obtained using Equation 1 might indicate small differences in the energy partitioning or reflects differences in the potential energy surface. From these results it is clear that the concerted elimination of halogen molecules is a direct process that takes place on a time scale faster than IVR. These observations



indicate that there is a time window of  $\sim 100$  fs to control the yield of these chemical reactions using a tailored laser pulse.

Inspired by the work of Shank and coworkers and Wilson and coworkers on the enhancement of three-photon excitation using chirp (55, 109, 110), we have explored the effect of chirp on the multiphoton excitation of  $\text{CH}_2\text{I}_2$  with 312-nm laser pulses (56). The product-state distribution (electronic, vibrational, rotational, and translational) resulting from the photodissociation of polyatomic molecules depends upon the potential energy surfaces participating in the fragmentation process, along with their couplings and the characteristics of the incident electromagnetic field (111). The field is characterized by its frequency, duration, intensity, and chirp. Chirp is caused by the propagation of laser pulses through matter that leads to group velocity variations as a function of frequency within the pulse, thus causing a frequency sweep (112, 113). In most cases, the group velocity variation causes a positive chirp in which the leading edge of the pulse is red-shifted and the trailing edge is blue-shifted with respect to the central frequency of the pulse. Negative chirp corresponds to the opposite effect. Increases in absolute chirp lead to a temporal broadening of the pulse and are usually considered detrimental for the study of ultrafast phenomena, in which the best time resolution is required.

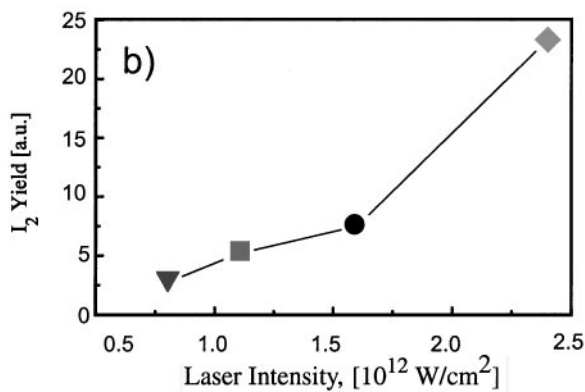
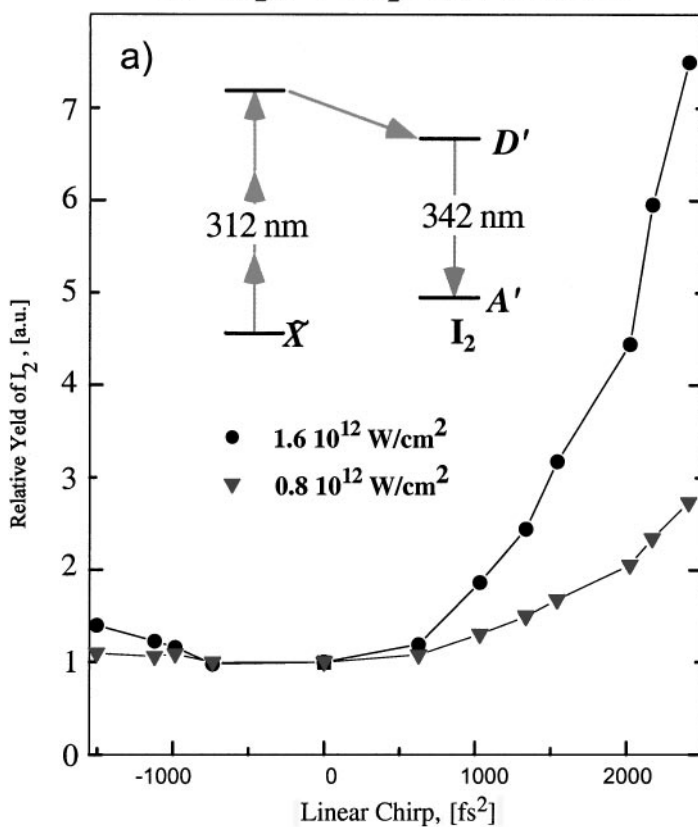
The shape and time evolution of a wave packet  $\psi(t)$  produced through absorption of an ultrafast laser pulse are determined by the phase factors in the following expression:

$$\psi(t) = \sum_n a_n e^{-iE_n t/\hbar} \varphi_n, \quad 2.$$

where  $E_n$  and  $\varphi_n$  denote the eigenvalue and eigenfunctions of each eigenstate  $n$ . The coefficient  $a_n$  is given by  $a_n = b_n e^{i\phi_n}$ , where  $b_n$  depends on the Franck-Condon overlap between the initial state and each final state  $n$ . The phase  $\phi_n$  depends on the linear chirp of the pulse,  $\phi''$ , where  $\phi_n = \frac{1}{2}\phi''(\omega_n - \omega)^2$ ,  $\omega_n = (E_n - E_o)/\hbar$  is the transition frequency of level  $n$ , and  $\omega$  is the carrier frequency of the laser pulse. The initial phase factor of each coefficient is equal for all states when excitation takes place with transform limited pulses, that is,  $\phi'' = 0$ . Therefore, the shape and dynamics of the wave packet can be controlled with the goal of affecting the outcome of a chemical process using chirped pulses.

Figure 3 presents the yield of the molecular pathway determined by detection of  $\text{I}_2 D' \rightarrow A'$  fluorescence intensity as a function of chirp. Increasing the chirp enhances the photodissociation yield significantly (56). The molecular pathway enhancement is found to be nonsymmetric for high fields, favoring positive over negative chirps. For example, the enhancement for  $\phi'' = -1500 \text{ fs}^2$  is 1.2, whereas for  $+1500 \text{ fs}^2$  it is 3.2 (see black circles in Figure 3). This observation implies that the observed enhancements are not due to pulse width effects, but they depend on the magnitude and sign of the linear chirp. The two scans shown in Figure 3a were obtained under identical conditions except for the intentional changes in the pulse intensity from  $0.8 \times 10^{12}$  to  $1.6 \times 10^{12} \text{ W/cm}^2$  (calculated for zero chirp pulses). The data are shown normalized to laser pulse energy (such that the yield

### Quantum Control of Yield The $\text{CH}_2\text{I}_2 \rightarrow \text{CH}_2 + \text{I}_2(\text{D}')$ reaction



for the transform-limited pulses equals unity) but are not corrected for the change in peak intensity caused by pulse broadening as a function of chirp. The effect of laser intensity on these control experiments is shown in Figure 3*b*, where the molecular pathway yield is shown to increase for positive 2400 fs<sup>2</sup> chirp by factors of 3 to 24 as the intensity of the laser pulses is increased from  $0.8 \times 10^{12}$  to  $2.4 \times 10^{12}$  W/cm<sup>2</sup>.

Considerable differences were observed between the dependence of the molecular pathway yield on laser pulse chirp depending on the central wavelength of the excitation pulse (56). For 624 nm, the yield of I<sub>2</sub>(D') was found to decrease with absolute chirp, whereas for 312 nm it increased. The probability of multiphoton transitions, in general, is proportional to the peak intensity raised to the  $n^{\text{th}}$  power ( $I^n$ ), where  $n$  is the number of photons. Therefore, multiphoton excitation is expected to be maximized for transform-limited pulses. For 624 nm excitation, the maximum yield was found for a chirp of  $-500$  fs<sup>2</sup>; however, for 312 nm the maximum yield was found for a chirp of 2400 fs<sup>2</sup> (56). Based on a peak intensity argument, the transition probability for the three-photon transition and hence the yield would have been expected to decrease by one order of magnitude because the pulse width triples at this chirp value.

The effects caused by chirp in the excitation pulses reflect characteristics of the potential energy surfaces and the nascent wave packet dynamics. For diatomic I<sub>2</sub>, Cao et al explained their observed chirp effects based on quantum mechanical calculations that show a "wave-packet following" effect for positive chirp (110). The potential energy surfaces of CH<sub>2</sub>I<sub>2</sub> are not known, which prevents us from giving an accurate quantum mechanical description of the effect. In principle, a similar wave-packet following effect could be responsible, given that the first photon transition is resonant, as in the I<sub>2</sub> experiment from Wilson's group (55).

## FREE-BOUND BIMOLECULAR REACTIONS: PHOTOASSOCIATION

Bimolecular reactions have proven to be extremely difficult to study using time-resolved methods because an encounter between two reagents is required. In the gas phase these encounters occur at random times, with random configurations and

---

**Figure 3** (a) Experimental measurement of the yield of the concerted elimination pathway producing I<sub>2</sub>(D') from the multiphoton dissociation of CH<sub>2</sub>I<sub>2</sub> using 312 nm laser pulses as a function of chirp. Results at two different intensities are shown. The insert shows the relevant energetics of the reaction. (b) Maximum I<sub>2</sub>(D') yield enhancement recorded at 2400 fs<sup>2</sup> chirp as a function of laser peak intensity. In all cases, the peak intensity was measured for zero chirp. Yields were normalized to unity for each laser intensity when the pulses were not chirped.

random energies. The experimental challenge is to devise ways to determine or restrict the initial collision conditions, such as impact parameter, orientation, collision energy, and time of collision. Traditional methods for studying bimolecular reactions include the use of molecular beams where the energy of the reactions can be regulated and special detectors to track the energy and position of the products (80, 81, 114, 115).

A number of methods have been proposed to obtain a detailed understanding of a bimolecular encounter. The interpretation of unimolecular dissociation reactions as the “half collision” is one such effort based on the principle of microscopic reversibility (116). According to this interpretation, a unimolecular photodissociation is equivalent to the second half of a full collision. The first half would involve the collision of the fragments. Clearly, only very specific initial conditions, such as impact parameter and reagent energies, would reproduce the observed dissociation dynamics. Therefore, unimolecular dissociation provides detailed information that is relevant to a very small subset of the possible bimolecular pathways.

Brooks et al used laser excitation during reactive collisions to study the transition states of chemical reactions (117). In their study, a nanosecond laser, not resonant with the asymptotic transitions of reactants or products, was used to open a chemiluminescent product channel; this was perhaps one of the first attempts to change the course of a bimolecular reaction by excitation of the transient collision complex. A different approach to the study of bimolecular reactions with ultrafast pulses takes advantage of van der Waals clusters involving the two precursors (118–122). These clusters, formed in a supersonic jet expansion, are cooled into the most energetically stable configuration, thereby reducing the range of initial reaction parameters. Essentially, the bimolecular encounter is converted into a unimolecular dissociation; therefore, the collision geometry is restricted, and with it the impact parameter. Laser excitation liberates one of the reagents or excites one of the reagents to a reactive state in order to initiate the reaction. The laser determines the available energy and the time of collision. These studies have been carried out using frequency (119) as well as time-resolved methods (118, 120–122). The computation of time-dependent dynamics in excimer molecules formed from van der Waals clusters has been considered by Petsalakis et al (123).

A method that has emerged as a new possibility in the study of bimolecular reactions is femtosecond photoassociation spectroscopy (99, 124–126). The photoassociation process, involving cooperative absorption of a photon by a pair of unbound atoms or molecules, causes bond formation between them in a free-to-bound photonic transition. Although photoassociation has been known at least since 1937 (127), the chemical implications of this process were described conceptually much later by Dubov et al (128). Photoassociation has been used for the spectroscopic study of excimer and exciplex molecules that have a repulsive ground state (129–138) and more recently has gained interest because of its role in the generation of ultracold molecules (139–153), the real time observation of bimolecular reactions (124, 154), and control of bimolecular encounters (99, 126, 155).

Even though most of the work in the area of laser control of chemical reactions has been dedicated to unimolecular processes (20, 156), some groups have begun to investigate how to control bimolecular reactions (157–160). The yield of a bimolecular reaction is determined by the energy of the collision, relative orientation of the reactants, and impact parameter of the encounter. The photoassociation process has been demonstrated to achieve control of these three key parameters (99, 126). Short-pulse photoassociation provides a well-determined initiation time for the reaction as well as an alignment with respect to the laboratory frame. These additional parameters allow for very detailed studies of bimolecular chemical reactions. Studies from our group have established that photoassociation is possible with femtosecond laser pulses, bringing the technique to the time scale of vibrational motion ( $10^{-14}$ – $10^{-12}$  s) (124, 126). The goal of our work has been to perform time-resolved measurements of transition state dynamics during reactive bimolecular collisions, to demonstrate control over the impact parameter of bimolecular reactions, and to establish the dependence of the photoassociation process on different laser characteristics (duration, frequency, and chirp) in order to explore the optimum balance between wavelength selectivity and temporal resolution. In Figure 4a a sketch of the photoassociation process  $\text{Hg} + \text{Hg} \rightarrow \text{Hg}_2^*$  is presented. The gray region represents the thermal population of free continuum states. Notice that resonance occurs only in a narrow range of internuclear distances, primarily at the “repulsive wall.” The binding wavelength is not absorbed by van der Waals clusters near the equilibrium distance or by the free reagents. The selectivity of the photoassociative process arises from the Franck-Condon overlap between the continuum wave functions in the ground electronic state and the bound wave functions of the upper state.

We have performed pump-probe experiments on the reaction  $\text{Hg} + \text{Hg} \rightarrow \text{Hg}_2^*$ , where a 312-nm pump pulse photoassociates a pair of ground state Hg atoms into the bound excited state  $\text{D}1_u$ . The fluorescence of the  $\text{Hg}_2 \text{D} \rightarrow \text{X}$  is collected as a function of the delay time between the pump and probe pulses as shown in Figure 4b for pulses that are polarized parallel and perpendicular to each other. For positive time delays, depletion of the  $\text{D}1_u$  state takes place as the molecules are excited to the  $1_g$  state by the probing pulse. The difference between both parallel and perpendicular transients indicates that the photoassociation process of this reaction is anisotropic with respect to the collision pair alignment. Because the pump laser is polarized, the nascent product molecules are aligned. This implies that a maximum in the depletion probability is expected for parallel pump-probe relative polarization (99). The fast onset of the depletion indicates that the photoassociation of free mercury atoms occurs within the laser pulse duration time. The large rotational distribution of the excimers leads to the dephasing of the rotational coherence. In that way, the rotational anisotropy decay depends on the rotational distribution parameters: the central quantum rotational level,  $j_{\text{max}}$ , and the range  $\Delta j$ . When a rotational distribution model is adopted,  $j_{\text{max}}$  and  $\Delta j$  can be obtained from a numerical fitting of the experimental rotational anisotropy, indicating that the photoassociation products have a narrow rotational distribution. The rotational

level distribution of the products reflects the range of collisional impact parameters that contribute to the photoassociation process,  $b = j_{\max} \hbar / (\mu v)$ . Control of the range of the collisional impact parameter can be achieved with the wavelength of the binding pulse through the Franck-Condon dependence of the photoassociation process (99, 126), which in turn determines the rotational excitation of the products. The results obtained for photoassociation at 312 nm (shown in Figure 4c) yield a rotational distribution with  $j_{\max} \approx 30$  and  $\Delta j = 90$  based on a Gaussian distribution model. From this we can estimate the most probable impact parameter to be  $b \approx 0.6 \text{ \AA}$ . The experimental results are in agreement with the quantum dynamics calculations of Backhaus & Schmidt (154). The most probable impact parameter for hard-sphere collisions in the absence of photoassociation is  $b \approx 3.2 \text{ \AA}$ . The difference in the impact parameter for the photoassociation at 310 nm and hard-sphere collisions indicates how the photoassociation process can be used to control the collision geometry and to limit the range of impact parameters.

Calculations of the photoassociation yield for a free-to-bound transition as a function of the pulse duration are shown in Figure 4d for different binding pulse wavelengths (155). In all cases the number of photons per laser pulse is kept constant, and a constant initial kinetic energy of the colliding atoms is assumed. The association yield features the following two interesting aspects. Starting from 100 fs and shorter pulse lengths, the yield shows a local maximum at approximately 10 fs for each laser wavelength. For increasing pulse length ( $\tau_{\text{pulse}} > 100 \text{ fs}$ ), the yield exhibits an additional maximum in the range from  $10^4$  to  $10^6 \text{ fs}$  for some laser frequencies. The enhancement of the association yield in the regime of ultrashort pulses can be readily explained by the following argument. For  $\tau_{\text{pulse}} \approx 10 \text{ fs}$ , the pulse spectrum overlaps almost the entire bond potential, resulting in an increase of the association yield. For even shorter pulse lengths, the energetic width exceeds the range of bound states, and the association yield decreases again. These competing effects lead to the maximum in the association yield at about 10 fs. For picosecond pulses ( $10^4$ – $10^5 \text{ fs}$ ), resonance with a free-to-bound transition for a certain final rovibrational level of the excited state leads to the enhancement of the photoassociation probability.

## BOUND-BOUND MOLECULAR TRANSITIONS: VIBRATIONAL DYNAMICS AND COHERENCE

Molecular dynamics are critically dependent on the inter- and intramolecular flow of energy. In the past decades there has been a considerable effort to measure and understand the flow of energy in the gas and condensed phases. The initial concepts of laser control of chemical reactions assumed that energy would remain localized in certain chemical bonds long enough to control reactivity (161–168). It was soon discovered that even for isolated molecules the energy dispersed among all accessible degrees of freedom in the picosecond time scale. Extensive studies carried out in the 1980s and 1990s on IVR processes and advances in ultrafast

lasers are combining to obtain a better understanding of these processes from small isolated molecules to large proteins in solution (169–171). Conceptually, the laser-sample interactions must take place in a time that is short compared to IVR (170). This concept is embodied in the pump-dump theory (16, 25). On the experimental front, the development of lasers with femtosecond pulse duration made the pursuit of this work possible (10, 62, 63, 65). Zewail's group quickly incorporated these techniques and dedicated their work to study the ultrafast dynamics of chemical reactions in the gas phase (172–174). The experimental observation of vibrational dynamics caused by impulsive excitation of multiple vibrational levels using femtosecond pulses in a pump-probe or in a TG arrangement provided experimental evidence of wave packet localization (9, 175–182). The ability to determine the position of a wave packet in time and space (within the constraint of the uncertainty principle) indicated that the pump-probe method is equivalent to the pump-dump technique (16, 25, 26) and could be used to control chemical processes (27, 28).

There are a number of successful laser techniques that have shown promise in schemes aimed at controlling chemical reactivity with lasers (e.g. pump-dump, interference of two or more pathways, and multiphoton excitation). All of these methods can be combined to achieve more general schemes for controlling chemical reactivity. Four-wave mixing with phase-matching detection is an ideal platform for the coherent combination of degenerate laser pulses. Phase-matching detection ensures that the signal arises from the coherent contribution of the laser beams without requiring active phase control. Our work on degenerate four-wave mixing (FWM) has shown that pulse sequences can be used to probe the vibrational dynamics of molecules in a specific electronic state and to control coherence and population transfer between different states (71, 73, 74, 183, 184). This work has been a combination of experimental observation and theoretical interpretation based on density matrix and wave packet simulations (73, 184, 185).

The FWM signal results from the polarization of the sample following three consecutive electric field interactions. The lasers and detector are arranged in a phase matching configuration that conserves energy and momentum. This ensures coherent interactions among the beams and determines the sign of the electric field interactions with the sample. Each electric field can be described by  $\vec{E}(t) = E(t)e^{i(\mathbf{k}\cdot\mathbf{x}-\omega t)} + \tilde{E}(t)^*e^{-i(\mathbf{k}\cdot\mathbf{x}-\omega t)}$ , where  $\tilde{E}(t)$  is the time-dependent amplitude of the field,  $\mathbf{k}$  is the wave vector,  $\mathbf{x}$  is the space coordinate of the sample and  $\omega$  is the carrier frequency of the laser. Because of the geometrical arrangement, the contribution of beams  $E_a$  and  $E_c$  always carry a positive wave vector, and beam  $E_b$  a negative one (see Figure 1). The pulse sequence can be chosen to obtain different nonlinear optical processes. For example, the pulse sequence with the temporal order  $\exp[i(\mathbf{k}_1\mathbf{x} - \omega t_1)]$ ,  $\exp[-i(\mathbf{k}_2\mathbf{x} - \omega t_2)]$ , and  $\exp[i(\mathbf{k}_3\mathbf{x} - \omega t_3)]$ , is known as virtual echo (186), whereas the pulse sequence with the temporal order  $\exp[-i(\mathbf{k}_1\mathbf{x} - \omega t_1)]$ ,  $\exp[i(\mathbf{k}_2\mathbf{x} - \omega t_2)]$ , and  $\exp[i(\mathbf{k}_3\mathbf{x} - \omega t_3)]$ , is known as stimulated photon echo (15). Notice that each beam interacts only once with the molecules and that one is able to determine the signs for the electric field

interactions within the constraints of the phase-matching detection geometry. This flexibility is not usually available with collinear pulses.

Here we illustrate how the time delay between the first two pulses can be used to control the FWM signal. The signal is proportional to the square of the average third-order polarization given by  $P^{(3)} = \text{Tr}[\hat{\rho}^{(3)}\hat{\mu}]$ , where  $\hat{\rho}^{(3)}$  is the third-order density matrix and  $\hat{\mu}$  the dipole moment operator. We derive simplified expressions for the density matrix elements with first- second-, and third-order dependence in the electric field interaction. This can be demonstrated with a simple model that includes two vibrational levels in the ground state and two in the electronically excited state. The vibrational levels are separated by  $\hbar\omega_g$  and  $\hbar\omega_e$  in the ground and excited states, respectively. The laser pulses are considered very short, such that their bandwidth is larger than  $\omega_g$  or  $\omega_e$ . The three pulses are degenerate and resonant with the electronic transition. The system is assumed to be at a temperature that allows the two ground state vibrational levels to be equally populated. After the first laser interaction the first-order density-matrix elements,  $\rho_{ij}^{(1)}(t)$ , depend on the sign of the interaction with the electric field. Interaction with  $e^{-i\omega t}$  yields a first-order electronic coherence (off-diagonal elements)

$$\rho_{eg}^{(1)}(t) \propto e^{-i\omega_e t}, \quad 3a.$$

where  $e, g$  denotes vibrational levels of the excited and ground state, respectively. Interaction with  $e^{i\omega t}$  yields

$$\rho_{ge}^{(1)}(t) \propto e^{i\omega_e t}. \quad 3b.$$

Population transfer occurs upon interaction with the second laser pulse. The resulting expression contains the population of the four levels. Notice that populations (diagonal elements) are time independent when no relaxation is included (as in this model). The simplified second-order density-matrix elements are given by the populations

$$\rho_{gg}^{(2)}(t) \propto -A \cos(\omega_e \tau_{12}/2), \quad 4a.$$

$$\rho_{ee}^{(2)}(t) \propto A \cos(\omega_g \tau_{12}/2), \quad 4b.$$

and the vibrational coherences

$$\rho_{g'g}^{(2)}(t) \propto -A \cos(\omega_e \tau_{12}/2)e^{-i\omega_g t}, \quad 4c.$$

$$\rho_{e'e'}^{(2)}(t) \propto A \cos(\omega_g \tau_{12}/2)e^{i\omega_e t}, \quad 4d.$$

where the time delay between the first two laser pulses is  $\tau_{12}$ , and  $A$  is a constant that depends on the laser intensity and the transition dipole moment. The primes indicate different vibrational levels in each electronic state. The dependence on



$\tau_{12}$  is manifested as well in the third-order density matrix expression for a virtual echo pulse sequence,

$$\begin{aligned} \rho_{eg}^{(3VE)}(t) \propto e^{-i\omega(t - (\tau_{13} - \tau_{12}))} [\cos(\omega_g \tau_{12}/2) \cos(\omega_e \tau_{23}/2) \\ + \cos(\omega_e \tau_{12}/2) \cos(\omega_g \tau_{23}/2) e^{i\varphi_{eg}}], \end{aligned} \quad 5.$$

where the phase is given by  $\varphi_{eg} = (1 + (-1)^{(e+g)})\omega_g \tau_{13}/2$ . Notice that the third-order matrix elements achieve their maximum before the third pulse is applied, when  $t = \tau_{13} - \tau_{12}$ , hence the name virtual echo (186). From Equation 5 we can distinguish two oscillatory components as a function of the scanning time  $\tau_{23}$ ; one oscillates with  $\omega_e$ , reflecting excited-state dynamics and the other with  $\omega_g$ , reflecting ground-state dynamics. The molecular response for a virtual echo process can be expressed diagrammatically by using two double-sided Feynman diagrams (see Figure 5a),  $R_1$  and  $R_4$ , corresponding to excited-state and ground-state dynamics, respectively (13–15, 185). The amplitude of each response function is controlled by the fixed time delay  $\tau_{12}$ . Note that the parameter  $\tau_{12} = 2\pi(n + 1/2)/\omega_e$ , where  $n$  is an integer, can be used to cancel the  $R_4$  response (see Equation 5). These values for  $\tau_{12}$  would cancel the observation of ground-state dynamics as a function of  $\tau_{23}$ . Notice that a similar condition exists for  $\tau_{12} = 2\pi(n + 1/2)/\omega_g$  for canceling the excited-state contribution. The time delay between the first two pulses can be set such that two wave packets formed from the ground state vibrational levels interfere destructively, leading to the cancellation of the excited-state contribution (185). The control mechanism in a stimulated photon echo pulse sequence is apparent from the third-order density matrix elements,

$$\begin{aligned} \rho_{eg}^{(3SPE)}(t) \propto e^{-i\omega(t - (\tau_{13} + \tau_{12}))} [\cos(\omega_g \tau_{12}/2) \cos(\omega_e \tau_{13}/2) \\ + \cos(\omega_e \tau_{12}/2) \cos(\omega_g \tau_{13}/2) e^{i\varphi_{eg}}]. \end{aligned} \quad 6.$$

Notice that the matrix element achieves its maximum at  $t = \tau_{13} + \tau_{12}$ . The stimulated photon echo technique offers two possibilities for control of the intramolecular dynamics. In one case, the time delay  $\tau_{12}$  is fixed (scanning time  $\tau_{23}$ ); in the other case, the time delay  $\tau_{13}$  is fixed (scanning time  $\tau_{12}$ ). The latter has been called mode suppression (187, 188). For both cases we can distinguish two oscillatory components as a function of the scanning time; one oscillates with  $\omega_e$ , and the other with  $\omega_g$ . The contribution of each component is controlled by the fixed time delay,  $\tau_{13}$  or  $\tau_{12}$ , allowing the control of molecular responses  $R_2$  and  $R_3$ , respectively (see Figure 6a).

The coherent nature of FWM experiments provides the opportunity to harness the coherent properties of lasers for controlling intra- and intermolecular degrees of freedom. We have been exploring FWM methods in our group to achieve coherent control of molecular dynamics (71, 74, 183, 184) and illustrate this work with the following example. The data in Figure 5b were obtained with molecular iodine. The time delay between the first two pulses was fixed to be 460 fs (left transient)

# Coherent Control of Excited and Ground Vibrational Wave-packets

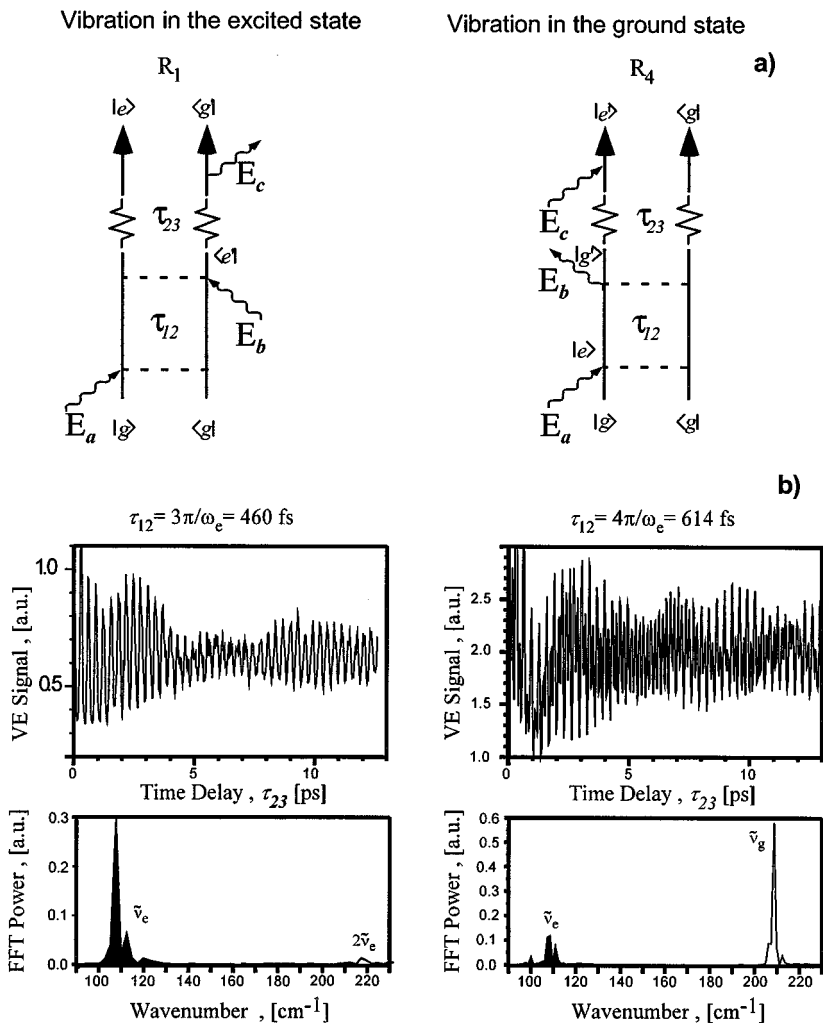


**Figure 5** (a) Double-sided Feynman diagrams of the experimental processes observed. The response functions  $R_1$  and  $R_4$  are responsible for the observation of excited- and ground-state intramolecular dynamics, respectively. (b) Experimental FWM data on molecular iodine obtained for pulse-sequences with a fixed time-delay between the first two pulses. The signal corresponds to a virtual photon echo pulse sequence. For the left-side transient, the delay time  $\tau_{12}$  was fixed at 460 fs, one and a half vibrational periods of the excited state of iodine. The observed vibrations have a period of 307 fs, corresponding to the excited-state vibrational motion. The power FFT (*bottom left*) shows that the main contribution is at  $108 \text{ cm}^{-1}$  corresponding to excited-state vibrational motion. For the right-side transient the delay time  $\tau_{12}$  was fixed at 614 fs, two vibrational periods in the excited state of iodine. The observed dynamics have a period of 160 fs, corresponding to ground state vibrations. The power FFT (*bottom right*) shows a main contribution at  $208 \text{ cm}^{-1}$  corresponding to ground-state vibrations and a smaller component at  $110 \text{ cm}^{-1}$  that corresponds to excited-state vibrations.

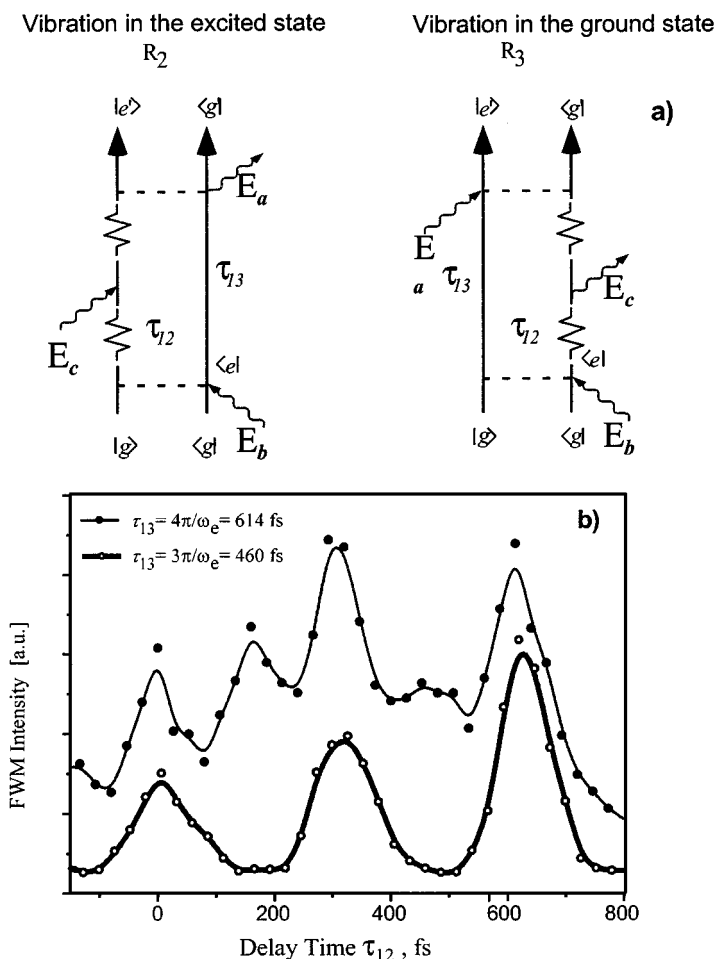
or 614 fs (right transient). The signal for  $\tau_{12} = 460$  fs can be assigned to the dynamics of the excited state with an oscillation period of  $\tau_e = 307$  fs corresponding to vibrational levels  $\nu' = 6-11$ . No evidence of ground-state dynamics is apparent in this transient or in the corresponding fast Fourier transform (FFT). For  $\tau_{12} = 614$  fs, the signal oscillates with  $\tau_g = 160$  fs, corresponding to the molecular dynamics in the ground state for vibrational levels  $\nu'' = 2-4$ . The FFT of these data confirms the predominant ground-state contribution.

The mechanism for signal emission corresponding to the ground-state transient can be understood in terms of a coherent Raman scattering process. The second pulse creates a coherent superposition of vibrational states in the ground state. This process is enhanced when the time between the first and second pulses matches the vibrational period of the excited state (71, 183, 184, 189, 190). The third laser pulse probes the resulting ground-state vibrational coherence. Coherent control over the ground- and excited-state vibrational wave packets is achieved by a combination of pump-dump and interference methods. When the time delay is set at  $\tau_{12} = 460$  fs, the transfer of the excited state superposition of states to the ground state cannot take place. This cancels the contribution from  $R_4$ , leaving only  $R_1$ . Probing with pulse  $E_3$  results in the observation of an excited-state vibrational coherence. The wave-packet representation of this process has been given by Pastirk et al (73, 204). Chen et al have shown that by using different color lasers they are able to detect the Stokes and anti-Stokes coherent Raman scattering and hence collect ground- and excited-state dynamics (191). Control over ground- or excited-state dynamics has been recently shown by Motzkus and coworkers using an adaptive pulse shaper with a learning algorithm (192). By detecting the photoelectron signal, Zanni et al have developed a very sensitive method to detect the ground-state dynamics observed after the second pulse (193).

Shank's group introduced a method aimed at suppressing the contribution of excited-state vibrational dynamics in order to improve relaxation rate measurements in liquids (187, 188, 194). They observed that when  $\tau_{13}$  is in phase with the excited-state dynamics,  $\tau_{13} = 2\pi n/\omega_e$  (mode suppression is on), the amplitude of the excited-state vibrations was greatly reduced. When  $\tau_{13}$  was out of phase (mode suppression is off), the excited-state vibrations were very prominent (187, 188).

We have explored control of the response functions responsible for stimulated photon echo signals (68). For these measurements the time delay  $\tau_{13}$  was kept fixed while the time  $\tau_{12}$  was scanned. Based on the literature (187, 188), mode suppression should take place when  $\tau_{13}$  is in phase with the vibrational motion of the excited state, 614 fs for gas-phase iodine, and mode suppression should not take place when the time delay  $\tau_{13}$  is out of phase, here 460 fs. In Figure 6*b* we present measurements for these cases on gas-phase molecular iodine. When  $\tau_{13} = 460$  fs, mode suppression is off and the data show pronounced 307 fs vibrations corresponding to the excited state without background or ground-state contributions. This is consistent with liquid-phase observations (188). The data obtained for  $\tau_{13} = 614$  fs, when mode suppression is on, show a considerable background signal as well as ground- and excited-state vibrational dynamics. The two transients in

## Stimulated Photon Echo and Mode Suppression



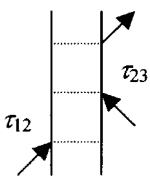
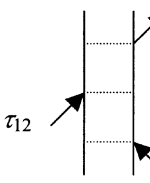
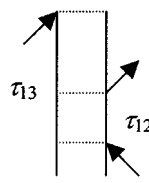
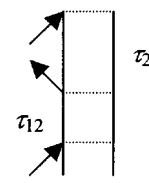
**Figure 6** Stimulated photon echo measurements on gas-phase molecular iodine when the delay time between the first and last pulses is fixed and the second pulse is scanned between them. (a) Double-sided Feynman diagrams describing the Liouville pathways that contribute to the signal arising from this method. Molecular responses  $R_2$  and  $R_3$  correspond to the excited- and ground-state vibrational motion, respectively. (b) Four-wave mixing (FWM) signal for two values of the fixed time  $\tau_{13}$ . When  $\tau_{13} = 460$  fs, the signal is modulated with a period of 307 fs (open circles), corresponding to the vibrational period of the excited state. When  $\tau_{13} = 614$  fs, the signal is modulated by 160 and 307 fs oscillations (filled circles), corresponding to a mixture of excited- and ground-state dynamics.

Figure 6b indicate that the background of the “mode suppressed” signal corresponds to a contribution that is independent of vibrational motion. However, excited- and ground-state vibrations are not suppressed in these measurements. When mode suppression is off, the molecular response known as  $R_2$  is canceled. When mode suppression is on, both  $R_2$  and  $R_3$  contribute to the signal. Mode suppression is useful in liquid phase studies because when mode suppression is on,  $R_3$  contributes a large signal that overwhelms the excited-state vibrational coherence.

We can summarize our work as follows: By selecting the fixed time delay between the pulses of different sequences we can control the different molecular responses. In this way, a molecular response can be canceled with specific time delays, as shown in Table 2 (71). Control over these response functions for a setup involving two pairs of collinear-phase locked pulses has recently been considered by Cina (195).

The previous example illustrates how the timing between the first two pulses can be used for control of the intramolecular dynamics (183, 184, 189). In a sense, the different pulse sequences can be thought of as optical analogues to multiple pulse NMR sequences (196, 197). The photon echo (PE) sequence is similar to the Hahn spin echo in NMR (198), and the stimulated photon echo is similar to the nuclear Overhauser effect spectroscopy method in NMR (199) (see Figure 7a). The cancellation of inhomogeneous broadening in PE measurements has been recognized since the first photon echo measurement in 1964 (200, 201). This advantage has been exploited to measure the homogeneous lifetime of complex systems such as large organic molecules in solution (72, 194, 202). Here we illustrate how this method works for molecular iodine.

**TABLE 2** Pulse sequence control of third-order response functions<sup>a</sup>

$R_1$	$R_2$	$R_3$	$R_4$
			
$\tau_{12} = 2\pi\left(n + \frac{1}{2}\right)/\omega_g$	$\tau_{12} = 2\pi\left(n + \frac{1}{2}\right)/\omega_g$	$\tau_{12} = 2\pi\left(n + \frac{1}{2}\right)/\omega_e$	$\tau_{12} = 2\pi\left(n + \frac{1}{2}\right)/\omega_e$
$\tau_{23} = 2\pi\left(n + \frac{1}{2}\right)/\omega_e$	$\tau_{13} = 2\pi\left(n + \frac{1}{2}\right)/\omega_e$	$\tau_{13} = 2\pi\left(n + \frac{1}{2}\right)/\omega_g$	$\tau_{23} = 2\pi\left(n + \frac{1}{2}\right)/\omega_g$

<sup>a</sup>The third-order response functions relevant to three-pulse four-wave mixing are given using double-sided Feynman diagrams (13–15). The time delays given correspond to the values that minimize the particular response function. The principle we have used is to make the pulses arrive out of phase with respect to the molecular dynamics. The maximum response for each response function can be achieved when the pulses arrive in phase with the molecular dynamics (when the factor of  $\frac{1}{2}$  is omitted).

Optical PE and spin echo processes are quite different phenomena. However, they have a large number of similarities. In the Hahn spin echo a coherent superposition of spins, originally pointed in the  $Z$ -axis, is rotated by 90 degrees into the  $XY$  plane. Inhomogeneous broadening in the sample causes dephasing of the coherent superposition as a function of time. Application of a  $\pi$  pulse causes an inversion in space, and hence the spreading motion becomes a focusing motion that leads to a rephasing of the original superposition. This generates the spin echo. The process can also be carried out by separating the  $\pi$  pulse into two  $\pi/2$  pulses, known as nuclear Overhauser effect spectroscopy. In the optical PE process the first electric field creates a coherence on the bra (see Equation 3b). After interaction with  $e^{i\omega t}$ , all the electronic coherences evolve with a positive sign while the relaxation process takes place. Subsequent  $e^{-i\omega t}$  interaction with two electric fields inverts the sign of the evolution, and the initial dephasing dynamics rephase to form an echo signal at  $\tau = 2\tau_{12}$  (see Equation 6). The main differences between spin echo and optical PE signals are the following: In spin echo the signal is proportional to the entire polarization of the system, whereas in PE the signal is proportional to the third-order polarization (which can be quite small). Therefore,  $\pi$  or  $\pi/2$  pulses that transform the entire population are not necessary to observe PE phenomena. In spin echo one usually works with a small number of levels, whereas in PE many more levels are available.

Experimental data for PE and reverse transient grating (RTG) measurements are shown in Figure 7b. In the pulse sequence for PE beam,  $E_b$  is followed by beams  $E_a$  and  $E_c$  overlapped in time ( $\mathbf{k}_S = -\mathbf{k}_1 + \mathbf{k}_2 + \mathbf{k}'_2$ ), whereas for RTG beam,  $E_c$  is followed by  $E_b$  and  $E_a$  overlapped in time ( $\mathbf{k}_S = \mathbf{k}_1 + \mathbf{k}_2 - \mathbf{k}'_2$ ). The differences observed in the background, undulation, and apparent signal-to-noise ratio in these data result from the difference in the first pulse interaction. When the first interaction is with  $e^{i\omega t}$ , action on the bra, the subsequent laser interactions lead to a cancellation of the inhomogeneous broadening in the sample and to the observation of the photon echo. When the first interaction is with  $e^{-i\omega t}$ , action on the ket, there is no mechanism to cancel the inhomogeneous contributions to the signal. The RTG data show a strong background and a slow undulation that results from the inhomogeneous rotational dephasing of the sample molecules. After the first 3 ps the RTG data show a mixture of ground- and excited-state dynamics. The observation of ground-state dynamics results from the initial thermal population of different vibrational modes. In the PE data only excited-state vibrational dynamics are observed.

In Figure 7c we present RTG and PE measurements for molecular iodine taken with long time delays. The measurements are taken as a function of temperature to illustrate the different mechanisms for coherence relaxation. Notice that the RTG measurements appear not to be temperature dependent in this temperature range (see Figure 7c). The reason for this observation is that the inhomogeneous contributions are caused by Doppler broadening, having a  $T^{1/2}$  dependence. In the PE measurements we can see that the homogeneous relaxation times are much longer and are found to decrease with temperature. The transients are fit by a single exponential decay. The single exponential behavior is consistent with the random nature of dephasing collisions, and hence the Poisson statistics. The cause for the decreased

coherence lifetime as a function of the temperature is the increase in the number density and hence an increase in the collision frequency. From these measurements a cross section for homogeneous vibronic relaxation,  $\sigma = 1150 \pm 150 \text{ \AA}^2$ , is obtained for iodine-iodine collisions (203). When the PE signal is recorded with higher temporal resolution vibrational and rotational features are revealed. The data in Figure 8*a* show that for PE the rotational coherence is maintained for hundreds of picoseconds. The transient shows the excited-state vibrational dynamics superimposed on the ground-state rotational coherence (Figure 8*b*). This combination is unexpected and may be the result of a macroscopic coherence (15, 204). The RTG data do not show the rotational and vibrational recurrences for time delays longer than 100 ps. Analysis of the Fourier transformed PE data (see Figure 8*c*) confirms that the vibrational coherence is due to the excited state.

The FWM signal contains valuable spectroscopic information, which can be extracted by detection with a spectrometer to obtain a signal as a function of three parameters,  $\tau_{12}$ ,  $\tau_{23}$ , and  $\omega_{eg}$  (73, 74, 184). Materny and coworkers have studied coherent anti-Stokes Raman scattering and degenerate FWM on iodine vapor (191, 205–208). Their data obtained using TG (positive time) and RTG (negative time) showed ground- or excited-state dynamics, depending on the detection wavelength (205, 209). In Figure 9*a*, we show a time-resolved, spectrally dispersed virtual echo transient obtained with transform-limited pulses for  $\tau_{12} = 460$  fs. Notice that all frequency components oscillate in phase with a period of 307 fs, corresponding to the excited-state vibrations. In order to explore the role of the pulse chirp in the control of the molecular dynamics, experimental data with  $\tau_{12} = 460$  fs were obtained when beams  $E_1$ ,  $E_2$ , and  $E_3$  were equally chirped,  $\phi'' = +3300 \text{ fs}^2$ . The bottom of Figure 9*b* shows the spectrally dispersed data for the above conditions. These data make it clear that chirped pulses lead to the formation of a chirped wave packet. The dotted lines correspond to the chirp of the laser and, as expected, the phase difference as a function of wavelength is imprinted on the wave packet (see Equation 2). The transient shows an increased contribution from the ground state (compare with upper plot). The mixing of both states' dynamics is evident in the anti-Stokes-shifted frequencies ( $\delta\tilde{\nu} > 0$ ), whereas the excited-state dynamics prevail in the Stokes frequencies ( $\delta\tilde{\nu} < 0$ ). Notice that the observed vibrations shift  $\approx 40$  fs for every  $100 \text{ cm}^{-1}$ , as expected from the introduced linear chirp. The complex dynamics observed following chirped pulse excitation could not be obtained from spectrally integrated transients.

## OFF-RESONANCE PROBING OF GROUND STATE DYNAMICS

When the bandwidth of a laser overlaps several rotational and/or vibrational states the impulsive limit, a coherent superposition of states, can be formed by off-resonance excitation and its time evolution can be probed. The transient grating (TG) method is based on this principle and has been used extensively by the groups

### Photon Echo Measurements: Electronic, Vibrational and Rotational Coherence

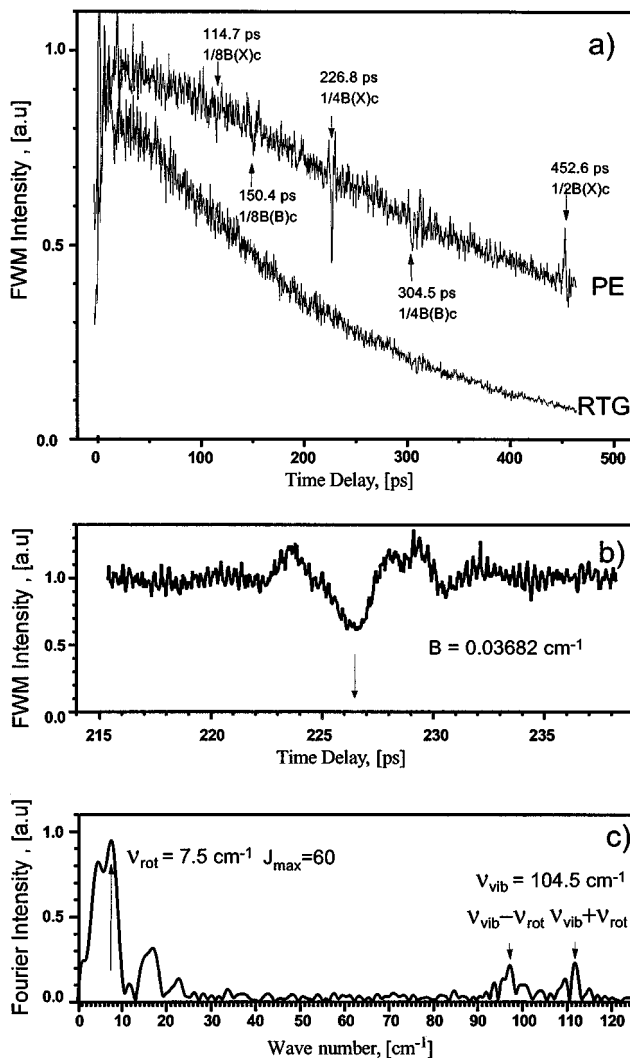


**Figure 8** (a) Experimental measurements of reverse transient grating (RTG) signal and photon echo (PE) signal obtained with high temporal resolution. The PE signal contains rotational recurrences, which can be assigned to the ground (X) and excited (B) states. (b) Higher temporal resolution of a section of the PE signal around the largest rotational recurrence at 226.8 ps. The oscillatory features with a period of 307 fs correspond to excited-state vibrations, whereas the rotational revival corresponds to the ground state. (c) Fourier transform of the PE signal, showing the rotational component at low frequencies and the rovibrational components at higher frequencies. No other features were observed at higher frequencies.



of Fayer and Nelson to explore molecular dynamics in gas and condensed phases (175, 210–212). The crossing of the two plane-wave beams forms a grating in the sample with regions of high and low polarization. The third laser Bragg-diffracts from the grating to generate the observed signal. The diffraction process is very similar to the diffraction of X-rays from crystalline systems because the spatial arrangement of the lasers leads to the spatial coherence in the sample. More recent work on off-resonance probing of gas phase samples includes the work of Chen and coworkers using Raman-induced polarization spectroscopy (213), as well as others (214, 215).

The homodyne detected off-resonance FWM signal can be classified as a coherent Raman scattering process. When the three incident lasers pulses are ultrafast, the impulsive limit, the impulsive coherent Raman scattering (ICRS) signal can be evaluated using the following expression (15)

$$S_{ICRS}(\tau) = |\chi_{\alpha\alpha}(\tau)|^2 \quad 7.$$

where

$$\chi_{\alpha\alpha}(\tau) \equiv -\frac{i}{\hbar} \langle [\alpha(\tau), \alpha(0)] \rho_g \rangle. \quad 8.$$

In Equation 8,  $\alpha$  is the electronic polarizability, and  $\rho_g$  represents the equilibrium ground-state density operator. Notice that the time-domain ICRS signal depends on the purely imaginary  $\chi_{\alpha\alpha}(\tau)$ , a quantity that depends on the response function associated with the electronic polarizability. For a system close to the classical limit, the imaginary part of any operator is proportional to time derivative of the full operator, therefore

$$\chi_{\alpha\alpha}(\tau) \cong \frac{1}{k_B T} \frac{d}{d\tau} \langle \alpha(\tau) \alpha(0) \rho_g \rangle. \quad 9.$$

This result comes from the fluctuation-dissipation theory (15). Where the time correlation function, the expression in the brackets in Equation 9, depends on two factors. First, only Raman active modes, those for which  $\partial\alpha/\partial q_j \neq 0$ , where  $q_j$  represents a given normal mode, can be observed. Second, only the Raman active modes whose frequencies lie within the spectral window of the laser pulses participate. The bandwidth restriction is not expressly written in Equation 9 because we have assumed the impulsive limit, hence infinite bandwidth. In the gas phase, changes in the polarizability are caused by rotational and vibrational motion of the molecules. Raman transitions with linearly polarized light depend on the polarizability operator,

$$\hat{\alpha} = \hat{\alpha}_0 + \hat{\gamma}_0 \frac{2}{3} P_2(\cos \theta), \quad 10.$$

where  $\hat{\alpha}_0$  and  $\hat{\gamma}_0$  are the isotropic and anisotropic components of the polarizability operator and  $P_2$  is the Legendre polynomial. The isotropic component gives the signal near time-zero delay of the scanning pulse; the anisotropic term gives the

signal for later times. The selection rule for linear molecules is  $\Delta J = 0, \pm 2$ . After interaction with two overlapped pulses the rotational wave packet consists of three types of coherent states with amplitudes that depend on  $\Delta J$ . For  $\Delta J = 0$  transitions, the alignment is time independent; therefore, these transitions do not contribute to the signal. Keeping only the  $\Delta J = \pm 2$  terms, the beating frequencies are  $\Omega_J^{+2} = (\varepsilon_{J+2} - \varepsilon_J)/\hbar$ ,  $\Omega_J^{-2} = (\varepsilon_J - \varepsilon_{J-2})/\hbar$ . Where the rotational energy levels are given by  $\varepsilon_J = [BJ(J+1) - DJ^2(J+1)^2]ch$ , with  $B$  the rotational constant and  $D$  the centrifugal distortion in wave numbers. If we assume  $\Omega_J^{+2} \approx \Omega_J^{-2} = \omega_J$  with  $\omega_J = 2\pi c[(4B - 6D^3)(J + 3/2) - 8D(J + 3/2)^3]$ , a situation that is true for large  $J$ , we obtain the following expression for the off-resonant signal:

$$S_{ICRS}(\tau) \propto \left| \sum_J n_J \omega_J \sin(\omega_J \tau) \right|^2, \quad 11.$$

where  $n_J$  represents the initial population of each rotational state defined by the Boltzmann distribution. Figure 10a depicts the initial alignment of the molecules at time zero, represented by a cosine-squared distribution from  $P_2(\cos \theta)$  in Equation 10. The broad rotational distribution causes fast rotational dephasing of the wave packet. Notice that the alignment is re-established after a time equivalent to  $(1/4Bc)$ , giving rise to a rotational recurrence or revival. Notice that a half recurrence is also depicted. Half recurrences can be observed whenever the contributions of odd and even  $J$  levels are unequal. The relative contributions are determined by the nuclear spin statistics. The signal is proportional to the square of the derivative of the time-dependent alignment; this function is depicted in the bottom of Figure 10a.

Figure 10b shows data for air, nitrogen, and oxygen. The experimental data are shown in black, and the simulations, using Equation 11, are shown as mirror images in red. From the data, it is clear that the rotational recurrence time for nitrogen is 4.15 ps and the rotational recurrence time for oxygen is 5.77 ps. Figure 10b shows that off-resonance probing is ideal to study mixtures, no wavelength tunability is required, and the signals from all components are separated by the differences in their rotational constants. Our results are in very good agreement with those of Chen and coworkers obtained using Raman-induced polarization spectroscopy (213, 217). It is particularly interesting when signals from two different species overlap. This situation is shown in Figure 10c. The sample is air, at a time delay at which oxygen and nitrogen recurrences overlap. Two simulations are given for these data. The first contains a sum of both signals squared, and the second contains the square of the sum of both contributions. The latter simulation gives the best fit to the data. Because the signal arises from the macroscopic polarization of the sample, it is proportional to the square of the sum of all anisotropic contributions; therefore, cross terms are expected. These data are valuable because they show that overlapping recurrences can be used to calibrate a time-domain spectrometer and to amplify the signal of a weak sample by mixing it with a strongly scattering sample. Hayden & Chandler used a pair of femtosecond

pulses with different wavelengths to coherently excite high vibrational overtones by a CARS process (225). A third laser pulse probed the grating generated by the first two pulses. These gas-phase measurements showed the early rotational dephasing of the molecular ensemble.

In the 1970s, Heritage et al used a picosecond transient birefringence method to observe the rotational recurrences of CS<sub>2</sub>, showing that time-resolved data can provide accurate rotational constants (218). Later, measuring polarized fluorescence from jet-cooled molecules, Zewail, Felker, and others have explored the molecular structure of large organic molecules and clusters using time-resolved rotational coherence spectroscopy (219–224).

In Figure 11, we show time-resolved, off-resonance TG measurements on CS<sub>2</sub> and benzene vapors. The CS<sub>2</sub> data (shown in Figure 11*a*) contain the initial rotational dephasing near time zero, two half-rotational recurrences at 38.2 and at 114.7 ps, and two full rotational recurrences at 76.5 and 152.4 ps. From these recurrences, a rotational constant of  $B = 0.10912 \pm 0.00002 \text{ cm}^{-1}$  and a centrifugal distortion of  $D = (6.4 \pm 0.2)10^{-9} \text{ cm}^{-1}$  can be determined. These constants are in very good agreement with the literature (226). The signal is found to decay owing to collisional dephasing. Figure 11*b* shows off-resonance, time-resolved, and spectrally dispersed FWM data for benzene. The signal, in this case, is detected with a spectrometer and a CCD detector, allowing frequency resolution. The initial features are the time-zero instantaneous polarizability response and the initial rotational dephasing. The following features correspond to the rotational recurrences. From these data, the rotational constant for benzene can be determined to be  $0.1897 \pm 0.0002 \text{ cm}^{-1}$ . This value is in excellent agreement with the literature value of  $0.1896 \text{ cm}^{-1}$  (227). The spectral information can be used to separate imperfections in the laser pulse, such as chirp from the molecular dynamics.

Experimental data on gas phase HgI<sub>2</sub> together with the theoretical simulation are shown in Figure 12. The transient consists of three contributions. At time zero there is a sharp feature corresponding to the isotropic instantaneous polarizability. This feature has no dependence on the intramolecular degrees of freedom and it is observed for all media, even for isolated atoms (13, 216). The data show a fast vibration that is modulated by a very low frequency envelope. The vibrations with a 211-fs period correspond to the symmetric stretch, the only Raman-active mode in this linear molecule (228). The slow modulation belongs to the anisotropic contribution to the signal that depends on the molecular orientation.

To model the data in Figure 12, we separate the isotropic and anisotropic contributions to the susceptibility (229). The vibrational motion makes the major contribution to the isotropic susceptibility. Based on the bandwidth of our laser pulse, only a few vibrational overtones are excited coherently. The anisotropic part of the susceptibility depends on the changes in orientation of the molecules caused by rotational motion, with some contribution from vibrational motion. There is an additional zero-time feature with amplitude  $A_z$  that arises from the equilibrium isotropic polarizability  $\alpha_0$ . The off-resonance transient-grating (TG)

## Ground State Rotational and Vibrational Dynamics

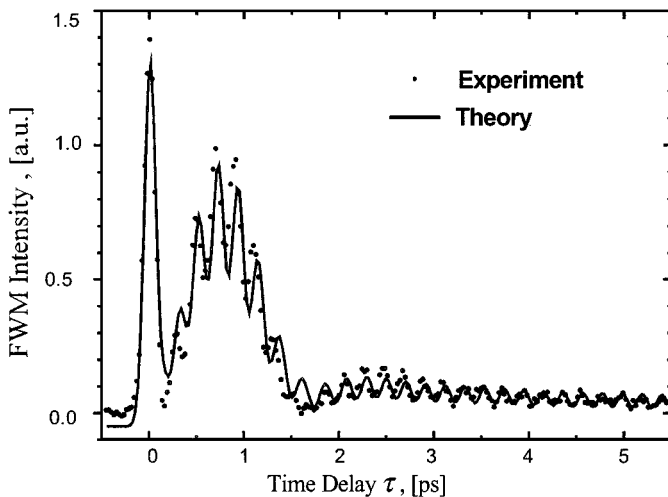


**Figure 12** Off-resonance transient-grating signal for  $\text{HgI}_2$ . The experimental transient (circles) is modeled using Equation 12 to obtain the theoretical simulation (solid line). The time-zero feature corresponds to the instantaneous polarizability. The fast vibrations, with a 211-fs period, correspond to the symmetric stretch, and the slow modulation corresponds to the rotational anisotropy.

signal for a molecular system in the gas phase with an active Raman vibrational mode is

$$S_v(\tau) = \left| A_Z \delta(\tau) + A_v e^{-(\tau/T_{2v})^2} \cos\left(\frac{1}{2}\omega_v \tau + \phi_{iso}\right) + A_{rot} \cos\left(\frac{1}{2}\omega_v \tau + \phi_{aniso}\right) \sum_J n_J \omega_J \sin(\omega_J \tau) \right|^2, \quad 12.$$

where the constants  $A_v$  and  $A_{rot}$  are the amplitudes of the time-zero vibrational and rotational components, respectively;  $\phi_{iso}$  and  $\phi_{aniso}$  are vibrational phases, and  $\omega_v$  is the vibrational frequency of the mode involved.  $T_{2v}$  represents the vibrational relaxation time. The first term represents the contribution of the instantaneous polarizability, and the second term represents the vibrational contribution, both caused by the isotropic component of the polarizability. Finally, the last term is related to the anisotropic polarizability, depending on the vibrational and rotational motions. Convolution of the simulation by the finite temporal width of our laser pulses yields the final result.

The simulation of the  $\text{HgI}_2$  data is shown in Figure 12 (circles) together with the experimental data (line). The data were simulated using Equation 12. In our model the three amplitude parameters, the phases, and the relaxation time were adjusted; all the other values were obtained from spectroscopic parameters (228, 230). The

relaxation time obtained from the simulation is  $T_{2v} = 20$  ps. It is clear that the model reproduces the most salient characteristics of the data. The small differences between model and data could be reduced by using a nonlinear least-squares fitting routine.

We have used the TG technique to explore the behavior of molecules in strong laser fields. Strong nonresonant laser fields from ultrafast laser pulses can cause very large electric-field gradients. Molecules experience a large torque along the polarization vector of the field owing to their anisotropic polarizability. With long laser pulses the torque is enough to cause adiabatic alignment (231, 232). However, with ultrafast pulses the torque provides an “instantaneous” kick towards alignment (233). For strong enough fields electronic state mixing can occur. When the electronic states have different geometry, this process leads to molecular deformation. Corkum and coworkers have combined intense off-resonance, chirped, circularly polarized fields to induce rotational acceleration and thus constructed a molecular centrifuge (234). For our measurements we use two high-intensity laser pulses followed by a weak probe pulse. The signal corresponds to the diffraction of the probe laser from the TG formed by the two intense pulses in the sample (216). The degree of molecular alignment and deformation are measured from changes in the rotational recurrences that are observed after field-free evolution of the molecular sample.

The full rotational recurrence of  $\text{CS}_2$  occurs at 76.5 ps, as seen in Figure 11a (216, 218). When the laser pulses are weak this feature can be observed, and an accurate rotational constant can be determined for the linear molecule (216, 218). In Figure 13a we show experimental data for the cases in which the first two laser pulses are one or two orders of magnitude stronger than the probe pulse. For low intensities the rotational recurrence can be modeled accurately by Equation 11. When the laser intensity of the first two pulses is increased by an order of magnitude the full rotational recurrence increases in intensity. The data shown in Figure 13a, when the laser intensity is  $10^{11}$  W/cm<sup>2</sup> (open squares), can be fitted by a room-temperature distribution of linear  $\text{CS}_2$  molecules. When the intensity is increased above  $10^{12}$  W/cm<sup>2</sup> the full rotational recurrence increases in intensity and changes shape [see Figure 13a (filled squares)]. Most markedly, the first feature at 76.1 ps becomes more intense than the second feature at 76.8 ps. The features observed at long time delays,  $>77.5$  ps, increase in intensity, and new oscillations are observed. This region of the transient is amplified by a factor of five in the figure (green trace). The high intensity data in Figure 13a are consistent with bending and stretching induced by the electric field. Roberts and coworkers (235) have recently studied electronic state mixing caused by high-intensity femtosecond laser excitation.

We have explored the use of off-resonance probing to study transients in flames. Figure 13b shows the changes caused by increasing the temperature of a sample. The data shown here were obtained for  $\text{CO}_2$  at room temperature and at 400°C. Notice that at higher temperatures the rotational coherence signal sharpens up and shifts slightly toward longer values. The narrowing is caused by the broader

### Off-Resonance FWM Measurements High Intensity and Temperature Effects

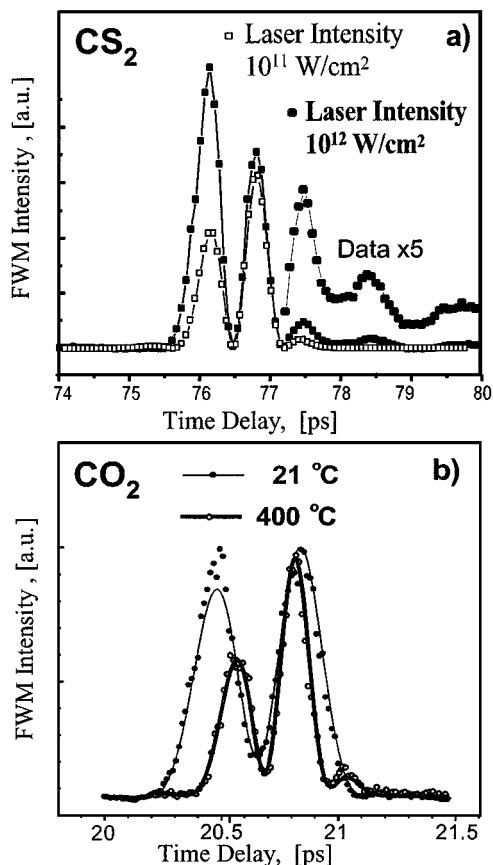


**Figure 13** (a) Effect of strong field intensity on the first full rotational recurrence of  $\text{CS}_2$ . Low laser intensity experimental data (open squares) are compared with high laser intensity data (filled squares) at room temperature. The transients were normalized to the laser intensity. A portion of the strong field transient is shown after a 5x amplification to highlight the additional features observed after 77 ps. (b) The effect of the temperature on the first full recurrence of  $\text{CO}_2$ . Experimental data are shown as dots and the simulations using Equation 11 are shown as lines. The room temperature ( $21^\circ\text{C}$ ) transient (filled circles) is compared with the high temperature ( $400^\circ\text{C}$ ) transient (open circles).

rotational distribution, and the shift toward longer times is caused by the centrifugal distortion. The main limitation of the TG technique as discussed here to study molecular species in flames is the faster collisional-dephasing time caused by the very fast translational motion.

Strong field laser excitation of atoms and molecules is an active area of research. Among the current topics of interest are generation of high harmonics, (236–242), above-threshold ionization (243–246), and plasma generation (247–249). The goal of these studies is usually to detect the high-order outcome of the interaction. Alternatively, one could explore the effects of strong fields on the sample. We have reviewed work from our group on a four-wave mixing (FWM) method to probe the sample after high-intensity laser interaction. This method provides high-resolution structural information and reports on changes induced by strong fields.

## CONCLUDING REMARKS

The quest to observe and control chemical reaction dynamics has been one of the most formidable scientific endeavors in physical chemistry since the nature of the chemical bond was uncovered (250). Progress over the past four decades has been astonishing: from the microsecond experiments of Porter (2, 3), to the indirect methods based on molecular beams (80, 81, 115, 251), and more recently, to the direct probing of the transition states of chemical reactions (252); we have witnessed a nine-order-of-magnitude improvement in time resolution. Many important lessons have been learned along the path of discovery. This review focuses on fundamental questions that are best studied in isolated systems, including concerted elimination chemical processes, bimolecular chemical reactions, wave packet dynamics, and molecules in strong fields. Regarding laser control, a number of schemes have been proven effective. Our approach has been to show that femtosecond time-resolved studies of isolated molecules provide crucial information regarding the best strategies for control.

Here we concentrate on the elimination of halogen molecules from dihalogenated alkanes. The experiments have shown that two bonds are broken and one is formed within 50 fs. The process has been shown to be faster than intramolecular vibrational relaxation and therefore it lends itself to relatively simple control schemes such as chirped laser excitation. There are a large number of chemical reactions thought to occur by concerted mechanisms. Improvements in time-resolved techniques would allow us to determine the precise chemical mechanism. The issue of concertedness is of importance in solution as well as in biological molecules. For example, the release of oxygen during the photosynthetic process is thought to proceed by a concerted process that avoids the formation of oxygen radicals (253–255).

The study of bimolecular reactions with the same level of detail and time resolution as unimolecular reactions remains a major challenge. We review work on

studies based on van der Waals clusters that serve as precursors for bimolecular reactions. More attention has been given to studies based on femtosecond photo-association. These studies promise to bring the powerful techniques being used to study unimolecular processes to bear on the rich dynamics involved in bimolecular reactions. These studies are challenging because they involve a larger number of chemical species that can interfere with the signals, and the concentration of collision partners is very small. The studies presented on the photoassociation of mercury atoms to form the excimer molecule are an important step in this direction (96, 124, 126, 154, 155, 256, 257).

We have reviewed the use of nonlinear optical methods like three-pulse four-wave mixing to measure dephasing times, to observe and to control rovibrational wave packets in the ground and excited states. The observation of vibrational and rotational wave packet dynamics by pump-probe methods has been reviewed previously. The pulse sequences in our FWM experiments combine the pump-probe concept and interference between quantum mechanical pathways to select the dynamics between the different Liouville pathways that yield signal. Therefore, with certain pulse sequences we are able to follow exclusively ground- or excited-state dynamics. These multiple pulse methods have some analogies with multiple pulse NMR. Extension of these third-order optical methods to fifth and higher orders is already under way following the theoretical work of Tanimura & Mukamel (258) and Ivanecky & Wright (259). Experimental results have already been obtained in some laboratories (260–272). The signal from some of the early measurements included cascading effects between third- and higher-order processes. In our work we have observed the cascading of a first-order process with a third-order process (273). This signal can be isolated with a specific pulse sequence that does not permit FWM to occur. The future goal of our studies is to control the wave-packet motion in molecules with multiple vibrational normal modes. These studies will seek to control the pathways for intramolecular vibrational energy redistribution with the goal of controlling reactivity. These methods can be applied to both ground and excited states.

Recent advances in laser technology allow the creation of extremely strong fields. Here we introduce off-resonance transient-grating techniques to study the effects of these high fields on molecules. Our experiments are relevant to the goals of controlling the external degrees of freedom of molecules with the purpose of focusing and aligning molecular beams using intense off-resonance fields (274, 275). Different regimes are observed, from perturbation of spectroscopic lines, to electronic state mixing, and finally to ionization.

In Figure 14 we seek to find some unifying concepts in the quest for laser observation and control of molecular dynamics. The roots of the tree identify some concepts and methods that have been introduced over the years based on the fundamental interactions of lasers and molecules. The trunk depicts the double-sided Feynman diagrams of the four Liouville paths that govern laser interactions with matter (up to fourth order). Here we find brave scientists taking these concepts and methods to apply them to the fundamental problems in physics, chemistry, and biology, as well as more applied disciplines such as computer science and medicine



# From Fundamental Concepts to Applications

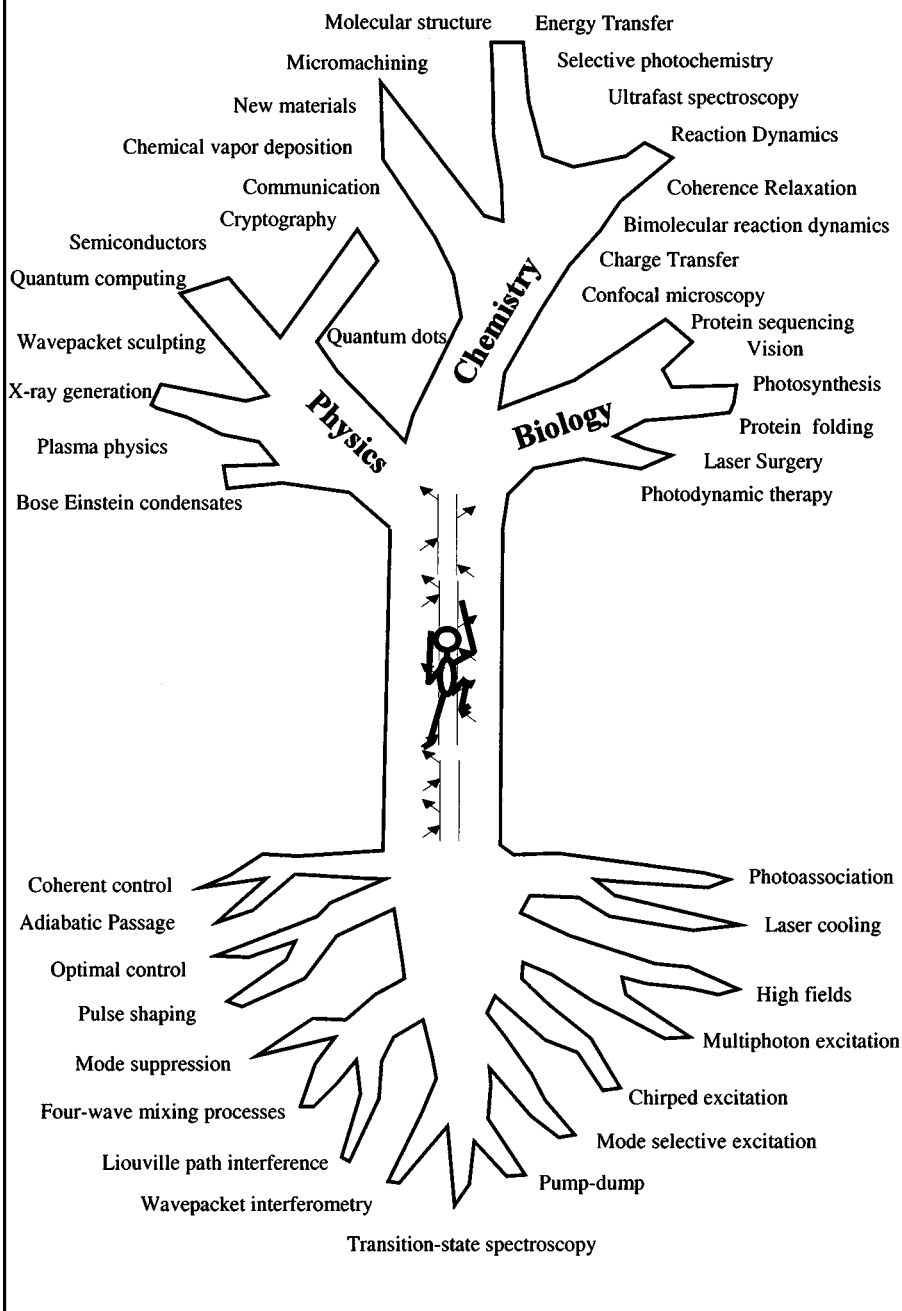


**Figure 14** Conceptual representation of the progress from fundamental ideas to applications in the major sciences and industry. See text for details.

and in industry. Many of the concepts in this tree are interrelated and can be associated with more than one discipline. Throughout the review, we reference the methods that we have used in our group's quest to take fundamental dynamics observations and use them for controlling molecular dynamics.

Advances in the past decade give definite hope for laser-controlled chemical processes. Progress will likely proceed along two lines. The first is the continued fundamental work on understanding the interaction of photons and molecules. The second is an industrial type of approach in which the main goal will be to find the optimum field to obtain a product. Both will continue to expand our knowledge and will allow us to deliver laser control to complex systems in which the Hamiltonian cannot be calculated. We hope this review stimulates a number of scientists and justifies continued funding of fundamental studies that will eventually lead to future applications.

## ACKNOWLEDGMENTS

It is a pleasure to acknowledge Shaul Mukamel, Jeff Cina, YJ Yan, and Gary Blanchard, Robert Cukier, James Harrison, and David Weliky for many stimulating discussions. The research presented here has been carried out by the following very talented students and postdocs: EJ Brown, M Comstock, BI Grimberg, P Gross, VV Lozovoy, U Marvet, I Pastirk, K Walowicz, and Q Zhang. This research was partially funded by a grant from the National Science Foundation (CHE-9812584). Major funding for our work came from a Lucille and David Packard Science and Engineering fellowship and an Arnold and Mabel Beckman Young Investigator award. The investment of these foundations on fundamental scientific discovery is gratefully acknowledged. MD is a Camille Dreyfus Teacher-Scholar and an Alfred P. Sloan Fellow. During the course of our research, EJ Brown was supported by a National Science Foundation Graduate Fellowship and I Pastirk by a James L Dye Endowment Fellowship.

**Visit the Annual Reviews home page at [www.AnnualReviews.org](http://www.AnnualReviews.org)**

## LITERATURE CITED

1. Hirschfelder JO, Eyring H, Topley B. 1936. *J. Chem. Phys.* 4:170–77
2. Porter G. 1950. *Discuss. Faraday Soc.* 9:60–82
3. Porter G, Ward B. 1965. *Proc. R. Soc. London* 287:457
4. Hochstrasser R, Kaiser W, Shank CV. 1980. In *Chemical Physics*, Vol. 14. Berlin: Springer-Verlag
5. Wiesenfeld JM, Greene BI. 1983. *Phys. Rev. Lett.* 51:1745–48
6. Taylor AJ, Erskine DJ, Tang CL. 1984. *Chem. Phys. Lett.* 103:430–35
7. Nuss MC, Zinth W, Kaiser W, Kolling E, Oesterhelt D. 1985. *Chem. Phys. Lett.* 117:1–7
8. Doany FE, Hochstrasser RM, Greene BI, Millard RR. 1985. *Chem. Phys. Lett.* 118:1–5
9. Rosker MJ, Wise FW, Tang CL. 1986. *Phys. Rev. Lett.* 57:321–24
10. Shank CV. 1986. *Science* 233:1276–80

11. Scherer NF, Knee JL, Smith DD, Zewail AH. 1985. *J. Phys. Chem.* 89:5141–43
12. Dantus M, Rosker MJ, Zewail AH. 1987. *J. Chem. Phys.* 87:2395–97
13. Shen YR. 1984. *The Principle of Nonlinear Optics*. New York: Wiley
14. Boyd RW. 1992. *Nonlinear Optics*. San Diego: Academic
15. Mukamel S. 1995. *Principles of Nonlinear Optical Spectroscopy*. New York: Oxford Univ. Press
16. Tannor DJ, Rice SA. 1985. *J. Chem. Phys.* 83:5013–18
17. Brumer P, Shapiro M. 1989. *Acc. Chem. Res.* 22:407–13
18. Shi S, Rabitz H. 1990. *J. Chem. Phys.* 92:364–76
19. Shapiro M, Brumer P. 1993. *J. Chem. Phys.* 98:201–5
20. Gordon RJ, Rice SA. 1997. *Annu. Rev. Phys. Chem.* 48:601–41
21. Shapiro M, Brumer P. 1986. *J. Chem. Phys.* 84:4103–4
22. Brumer P, Shapiro M. 1992. *Annu. Rev. Phys. Chem.* 43:257–82
23. Zhu LC, Kleiman V, Li XN, Lu SP, Trentelman K, Gordon RJ. 1995. *Science* 270:77–80
24. Zhu LC, Suto K, Fiss JA, Wada R, Seideman T, Gordon RJ. 1997. *Phys. Rev. Lett.* 79:4108–11
25. Tannor DJ, Kosloff R, Rice SA. 1986. *J. Chem. Phys.* 85:5805–20
26. Tannor DJ, Rice SA. 1988. *Adv. Chem. Phys.* 70:441–523
27. Bowman RM, Dantus M, Zewail AH. 1990. *Chem. Phys. Lett.* 174:546–52
28. Baumert T, Gerber G. 1994. *Isr. J. Chem.* 34:103–14
29. Baumert T, Thalweiser R, Weiss V, Gerber G. 1995. In *Femtosecond Chemistry*, ed. J Manz, L Wöste, pp. 397–432. Weinheim: VCH
30. Assion A, Baumert T, Helbing J, Seyfried V, Gerber G. 1996. *Chem. Phys. Lett.* 259:488–94
31. Averbukh IS, Vrakking MJJ, Villeneuve DM, Stolow A. 1996. *Phys. Rev. Lett.* 77:3518–21
32. Pausch R, Heid M, Chen T, Kiefer W, Schwöerer H. 1999. *J. Chem. Phys.* 110:9560–67
33. Yan YJ, Gillilan RE, Whitnell RM, Wilson KR, Mukamel S. 1993. *J. Phys. Chem.* 97:2320–33
34. Krause JL, Whitnell RM, Wilson KR, Yan Y, Mukamel S. 1993. *J. Chem. Phys.* 99:6562–78
35. Shi S, Woody A, Rabitz H. 1988. *J. Chem. Phys.* 88:6870–83
36. Judson RS, Rabitz H. 1992. *Phys. Rev. Lett.* 68:1500–3
37. Kosloff R, Rice SA, Gaspard P, Tersigni S, Tannor DJ. 1989. *Chem. Phys.* 139:201–20
38. Ruhman S, Kosloff R. 1990. *J. Opt. Soc. Am. B* 7:1748–52
39. Broers B, van den Heuvel HBV, Noordam LD. 1992. *Phys. Rev. Lett.* 69:2062–65
40. Melinger JS, Hariharan A, Gandhi SR, Warren WS. 1991. *J. Chem. Phys.* 95:2210–13
41. Band YB, Julienne PS. 1992. *J. Chem. Phys.* 96:3339–41
42. Band YB. 1994. *Phys. Rev. A* 50:5046–50
43. Cerullo G, Bardeen CJ, Wang Q, Shank CV. 1996. *Chem. Phys. Lett.* 262:362–68
44. Bardeen CJ, Wang Q, Shank CV. 1998. *J. Phys. Chem. A* 102:2759–66
45. Kohler B, Yakovlev VV, Che JW, Krause JL, Messina M, et al. 1995. *Phys. Rev. Lett.* 74:3360–63
46. Bardeen CJ, Che JW, Wilson KR, Yakovlev VV, Cong PJ, et al. 1997. *J. Phys. Chem. A* 101:3815–22
47. Papanikolas JM, Williams RM, Leone SR. 1997. *J. Chem. Phys.* 107:4172–78
48. Bardeen CJ, Che JW, Wilson KR, Yakovlev VV, Apkarian VA, et al. 1997. *J. Chem. Phys.* 106:8486–503
49. Zadayan R, Schwenter N, Apkarian VA. 1998. *Chem. Phys.* 233:353–63
50. Weinacht TC, Ahn J, Bucksbaum PH. 1998. *Phys. Rev. Lett.* 80:5508–11
51. Lozovoy VV, Antipin SA, Gostev FE, Titov

- AA, Tovbin DG, et al. 1998. *Chem. Phys. Lett.* 284:221–29
52. Lozovoy VV, Sarkisov OM, Vetchinkin AS, Umanskii SY. 1999. *Chem. Phys.* 243:97–114
53. Sarkisov OM, Tovbin DG, Lozovoy VV, Gostev FE, Antipin AA, Umanskii SY. 1999. *Chem. Phys. Lett.* 303:458–66
54. Bardeen CJ, Yakovlev VV, Wilson KR, Carpenter SD, Weber PM, Warren WS. 1997. *Chem. Phys. Lett.* 280:151–58
55. Yakovlev VV, Bardeen CJ, Che JW, Cao JS, Wilson KR. 1998. *J. Chem. Phys.* 108:2309–13
56. Pastirk I, Brown EJ, Zhang Q, Dantus M. 1998. *J. Chem. Phys.* 108:4375–78
57. Kleiman VD, Arrivo SM, Melinger JS, Heilweil EJ. 1998. *Chem. Phys.* 233:207–16
58. Legare F, Chelkowski S, Bandrauk AD. 2000. *J. Raman Spectrosc.* 31:15–23
59. Chelkowski S, Bandrauk AD. 1997. *J. Raman Spectrosc.* 28:459–66
60. Assion A, Baumert T, Bergt M, Brixner T, Kiefer B, et al. 1998. *Science* 282:919–22
61. Weinacht TC, White JL, Bucksbaum PH. 1999. *J. Phys. Chem. A* 103:10166–68
62. Fork RL, Greene BI, Shank CV. 1981. *Appl. Phys. Lett.* 38:671–72
63. Valdmanis JA, Fork RL, Gordon JP. 1985. *Opt. Lett.* 10:131–33
64. Valdmanis JA, Fork RL. 1986. *IEEE J. Quantum Electron.* QE22:112–18
65. Fork RL, Shank CV, Yen RT. 1982. *Appl. Phys. Lett.* 41:223–25
66. Kane DJ, Trebino R. 1993. *Opt. Lett.* 18:823–2567
67. Dantus M, Rosker MJ, Zewail AH. 1988. *J. Chem. Phys.* 89:6128–40
68. Wilhelm T, Piel J, Riedle E. 1997. *Opt. Lett.* 22:1494–96
69. Prior Y. 1980. *Appl. Opt.* 19:1741–43
70. Shirley JA, Hall RJ, Eckbreth AC. 1980. *Opt. Lett.* 5:380–82
71. Lozovoy VV, Pastirk I, Brown EJ, Grimberg BI, Dantus M. 2000. *Int. Rev. Phys. Chem.* 19:531–52
72. Vohringer P, Arnett DC, Yang TS, Scherer NF. 1995. *Chem. Phys. Lett.* 237:387
73. Pastirk I, Lozovoy VV, Grimberg BI, Brown EJ, Dantus M. 1999. *J. Phys. Chem. A* 103:10226–36
74. Lozovoy VV, Grimberg BI, Brown EJ, Pastirk I, Dantus M. 2000. *J. Raman Spectrosc.* 31:41–49
75. Zadoyan R, Apkarian VA. 2000. *Chem. Phys. Lett.* 326:1–10
76. Woodward RB, Hoffmann R. 1969. *Angew. Chem. Int. Ed. Engl.* 8:781–853
77. Dewar MJS. 1984. *J. Am. Chem. Soc.* 106:209–19
78. Borden WT, Loncharich RJ, Houk KN. 1988. *Annu. Rev. Phys. Chem.* 39:213–36
79. Strauss CEM, Houston PL. 1990. *J. Phys. Chem.* 94:8751–62
80. Bernstein RB. 1982. *Chemical Dynamics Via Molecular Beam and Laser Techniques*. New York: Oxford Univ. Press
81. Lee YT. 1987. *Agnew. Chem. Int. Ed. Engl.* 26:936–51
82. Butler LJ, Hints EJ, Shane SF, Lee YT. 1987. *J. Chem. Phys.* 86:2051–74
83. Wannemacher EAJ, Felder P, Huber JR. 1991. *J. Chem. Phys.* 95:986–97
84. Zewail AH. 1994. *Femtochemistry: Ultrafast Dynamics of the Chemical Bond*. Singapore: World Sci.
85. Pedersen S, Herek JL, Zewail AH. 1994. *Science* 266:1359–64
86. Kim SK, Pedersen S, Zewail AH. 1995. *J. Chem. Phys.* 103:477–80
87. Chachisvilis M, Fiebig T, Douhal A, Zewail AH. 1998. *J. Chem. Phys. A* 102:669–73
88. Fiebig T, Chachisvilis M, Manger M, Zewail AH, Douhal A, et al. 1999. *J. Phys. Chem. A* 103:7419–31
89. Folmer DE, Wisniewski ES, Castleman AW. 2000. *Chem. Phys. Lett.* 318:637–43
90. Catalan J, del Valle JC, Kasha M. 2000. *Chem. Phys. Lett.* 318:629–36
91. Baum G, Felder P, Huber JR. 1993. *J. Chem. Phys.* 98:1999–2010

92. Schwartz BJ, King JC, Zhang JZ, Harris CB. 1993. *Chem. Phys. Lett.* 203:503–8
93. Kwok WM, Phillips DL. 1995. *Chem. Phys. Lett.* 235:260–67
94. Kwok WM, Phillips DL. 1996. *J. Chem. Phys.* 104:2529–40
95. Marvet U, Dantus M. 1996. *Chem. Phys. Lett.* 256:57–62
96. Marvet U, Dantus M. 1996. See Ref. 173, pp. 134–37
97. Zhang Q, Marvet U, Dantus M. 1997. *J. Chem. Soc. Faraday Discuss.* 108:63–80
98. Marvet U, Zhang Q, Brown EJ, Dantus M. 1998. *J. Phys. Chem.* 109:4415–27
99. Marvet U, Zhang Q, Dantus M. 1998. *J. Phys. Chem. A* 102:4111–17
100. Zhang Q, Marvet U, Dantus M. 1998. *J. Chem. Phys.* 109:4428–42
101. Radloff W, Farmanara P, Stert V, Schreiber E, Huber JR. 1998. *Chem. Phys. Lett.* 291:173–78
102. Bergmann K, Carter RT, Hall GE, Huber JR. 1998. *J. Chem. Phys.* 109:474–83
103. Tarnovsky AN, Alvarez JL, Yartsev AP, Sundström V, Akesson E. 1999. *Chem. Phys. Lett.* 312:121–30
104. Marvet U, Brown EJ, Dantus M. 2000. *Phys. Chem. Chem. Phys.* 2:885–91
105. Dyne PJ, Style DWG. 1952. *J. Chem. Soc.* 1952: 2122–24
106. Style DWG, Ward JC. 1952. *J. Chem. Soc.* 1952: 2125–27
107. Okabe H, Kawasaki M, Tanaka Y. 1980. *J. Chem. Phys.* 12:6162–66
108. Duschek F, Schmitt M, Vogt P, Materny A, Kiefer W. 1997. *J. Raman Spectrosc.* 28:445–53
109. Berdeen CJ, Wang Q, Shank CV. 1995. *Phys. Rev. Lett.* 75:3410
110. Cao JS, Che JW, Wilson KR. 1998. *J. Phys. Chem. A* 102:4284–90
111. Hammerich AD, Kosloff R, Ratner MA. 1992. *J. Chem. Phys.* 97:6410–31
112. Treacy EB. 1969. *IEEE J. Quantum Electron.* 5:454
113. de Silvestri S, Laporta P, Svetlo O. 1984. *J. Quantum Electron.* QE20:533–30
114. Lee YT. 1982. In *Atomic and Molecular Beam Method*, ed. G Scoles, pp. 553–68. New York: Oxford Univ. Press
115. Herschbach DR. 1987. *Agnew. Chem. Int. Ed. Engl.* 26:1221–43
116. Atabek O, Lefebvre R. 1977. *J. Chem. Phys.* 67:4983–89
117. Brooks PR, Curl RF, Maguire TC. 1982. *Ber. Bunsenges Phys. Chem.* 86:401–7
118. Scherer NF, Khundkar LR, Bernstein RB, Zewail AH. 1987. *Chem. Phys.* 87:1451–53
119. Visticot JP, Soep B, Whitham CJ. 1988. *J. Phys. Chem.* 92:4574–76
120. Gruebele M, Roberts G, Dantus M, Bowman RM, Zewail AH. 1990. *Chem. Phys. Lett.* 166:459–69
121. Gruebele M, Sims IR, Potter ED, Zewail AH. 1991. *J. Chem. Phys.* 95:7763–66
122. Ionov SI, Brucker GA, Jaques C, Valachovic L, Witting C. 1993. *J. Chem. Phys.* 99:6553–61
123. Petsalakis ID, Mercouris T, Nicolaides CA. 1994. *Chem. Phys.* 189:615–28
124. Marvet U, Dantus M. 1995. *Chem. Phys. Lett.* 245:393–99
125. Marvet U, Dantus M. 1996. See Ref. 173, pp. 138–42
126. Gross P, Dantus M. 1997. *J. Chem. Phys.* 106:8013–21
127. Mrozowski S. 1937. *Z. Physik.* 106:458–62
128. Dubov VS, Gudzenko LI, Gurvich LV, Iakovlenko SI. 1977. *Chem. Phys. Lett.* 45:330–33
129. Bergeman T, Liao PF. 1980. *J. Chem. Phys.* 72:886–98
130. Inoue G, Ku JK, Setser DW. 1984. *J. Chem. Phys.* 80:6006–19
131. Ku JK, Setser DW, Oba D. 1984. *Chem. Phys. Lett.* 109:429–35
132. Rodriguez G, Eden JG. 1991. *J. Chem. Phys.* 95:5539–52
133. Schloss JH, Jones RB, Eden JG. 1992. *Chem. Phys. Lett.* 195–202
134. Jones RB, Schloss JH, Eden JG. 1993. *J. Chem. Phys.* 98:4317–34

135. Cline RA, Miller JD, Heinzen DJ. 1994. *Phys. Rev. Lett.* 73:632–35
136. Pavlenko VS, Nalivaiko SE, Egorov VG, Rzhavskii OS, Gordon EB. 1994. *J. Quantum Electron.* 24:199–206
137. Azinovic D, Li X, Milosevic S, Pichler G. 1996. *Phys. Rev. A* 53:1323–29
138. Gruber D, Li X, Windholz L, Gleichmann MM, Hess BA, et al. 1996. *J. Phys. Chem.* 100:10062–69
139. Thorsheim HR, Weiner J, Julienne PS. 1987. *Phys. Rev. Lett.* 58:2420–23
140. Miller JD, Cline RA, Heinzen DJ. 1993. *Phys. Rev. Lett.* 71:2204–7
141. Napolitano J, Weiner J, Williams CJ, Julienne PS. 1994. *Phys. Rev. Lett.* 73:1352–55
142. Williams CJ, Julienne PS. 1994. *J. Chem. Phys.* 101:2634–37
143. Moerdijk AJ, Verhaar BJ. 1995. *Phys. Rev. A* 51:R4333–36
144. Chapman MS, Ekstrom CR, Hammond TD, Rubenstein RA, Schmiedmayer J, et al. 1995. *Phys. Rev. Lett.* 74:4783–86
145. Band YB, Julienne PS. 1995. *Phys. Rev. A* 51:R4317–20
146. Lett PD, Julienne PS, Phillips WD. 1995. *Annu. Rev. Phys. Chem.* 46:423–52
147. Bahns JT, Stwaley WC, Gould PL. 1996. *J. Chem. Phys.* 104:9689–97
148. Vardi A, Abrashkevich D, Frishman E, Shapiro M. 1997. *J. Chem. Phys.* 107:6166–74
149. Wang H, Wang XT, Gould PL, Stwaley WC. 1997. *Phys. Rev. Lett.* 78:4173–76
150. Wang H, Gould PL, Stwaley WC. 1997. *J. Chem. Phys.* 106:7899–7912
151. Wang H, Stwaley WC. 1998. *J. Chem. Phys.* 108:5767–71
152. Gensemer SD, Gould PL. 1998. *Phys. Rev. Lett.* 80:936–39
153. Fioretti A, Comparat D, Crubellier A, Dulieu O, Masnou-Seeuws F, Pillet P. 1998. *Phys. Rev. Lett.* 80:4402–5
154. Backhaus P, Schmidt B. 1997. *Chem. Phys.* 217:131–43
155. Backhaus P, Schmidt B, Dantus M. 1999. *Chem. Phys. Lett.* 306:18–24
156. Gaspard P, Burghardt I. 1997. *Adv. Chem. Phys.* 101:491–581
157. Krause JL, Shapiro M, Brumer P. 1990. *J. Chem. Phys.* 92:1126–31
158. Potter ED, Herek JL, Pedersen S, Liu Q, Zewail AH. 1992. *Nature* 355:66–68
159. Brumer P, Shapiro M. 1997. *Adv. Chem. Phys.* 101:295–300
160. Apkarian VA. 1997. *J. Chem. Phys.* 106:5298–99
161. Letokhov VS. 1973. *Science* 180:451–58
162. Stone J, Goodman MF, Dows DA. 1976. *Chem. Phys. Lett.* 44:411–14
163. Mukamel S, Jortner J. 1976. *Chem. Phys. Lett.* 40:150–56
164. Letokhov VS, Makarov AA. 1978. *Appl. Phys.* 16:47–57
165. Quack M. 1978. *J. Chem. Phys.* 69:1282–1307
166. Quack M. 1979. In *Laser Induced Processes in Molecules*, ed. K Kompa, SD Smith, 6:142–44. Berlin: Springer-Verlag
167. Vander Wal RL, Scott JL, Crim FF. 1990. *J. Chem. Phys.* 92:803–5
168. Bar I, Cohen Y, David D, Rosenwaks S, Valentini JJ. 1990. *J. Chem. Phys.* 93:2146–48
169. Robinson PJ, Holbrook KA. 1972. *Unimolecular Reactions*. New York: Wiley
170. Zewail AH. 1980. *Phys. Today* 33:27–33
171. Manz J, Parmenter CS. 1989. *Chem. Phys.* 139:U1–U4
172. Manz J, Wöste L. 1995. *Femtosecond Chemistry*. Weinheim:VCH
173. Chergui M. 1996. *Femtochemistry: Ultrafast Chemical and Physical Processes in Molecular Systems*. Singapore: World Sci.
174. Sundström V. 1998. *Femtochemistry and Femtobiology*. Singapore: World Sci.
175. Yan Y-X, Cheng L-T, Nelson KA. 1987. In *Advances in Non-Linear Spectroscopy*, ed. RJH Clark, RE Hester, pp. 299–355. Chichester, UK: Wiley

176. Ruhman S, Williams LR, Joly AG, Kholer B, Nelson KA. 1987. *J. Phys. Chem.* 91:2237–40
177. Ruhman S, Joly AG, Nelson KA. 1987. *J. Chem. Phys.* 86:6563–65
178. Engel V, Metiu H, Almeida R, Marcus RA, Zewail AH. 1988. *Chem. Phys. Lett.* 152:1–7
179. Bowman M, Dantus M, Zewail AH. 1989. *Chem. Phys. Lett.* 161:297–302
180. Dantus M, Bowman RM, Zewail AH. 1990. *Nature* 343:737–39
181. Rosker MJ, Rose TS, Zewail AH. 1988. *Chem. Phys. Lett.* 146:175–79
182. Rose TS, Rosker MJ, Zewail AH. 1988. *J. Chem. Phys.* 88:6672–73
183. Brown EJ, Pastirk I, Grimberg BI, Lozovoy VV, Dantus M. 1999. *J. Chem. Phys.* 111:3779–82
184. Pastirk I, Brown EJ, Grimberg BI, Lozovoy VV, Dantus M. 1999. *Faraday Discuss.* 113:401–24
185. Grimberg BI, Lozovoy VV, Dantus M, Mukamel S. 2001. *J. Phys. Chem.* Submitted
186. Pshenichnikov MS, de Boeij WP, Wiersma DA. 1996. *Phys. Rev. Lett.* 76:4701–4
187. Schoenlein RW, Mittleman DM, Shiang JJ, Alivisatos AP, Shank CV. 1993. *Phys. Rev. Lett.* 70:1014–17
188. Bardeen CJ, Shank CV. 1993. *Chem. Phys. Lett.* 203:535–39
189. Knopp G, Pinkas I, Prior Y. 2000. *J. Raman Spectrosc.* 31:51–58
190. Materny A, Chen T, Schmitt M, Siebert T, Vierheilig A, et al. 2000. *Appl. Phys. B* 71:299–317
191. Chen T, Engel V, Heid M, Kiefer W, Knopp G, et al. 1999. *J. Mol. Struct.* 481:33–43
192. Hornung T, Meier R, Motzkus M. 2000. *Chem. Phys. Lett.* 326:445–53
193. Zanni MT, Davis AV, Frischkorn C, Elhanine M, Neumark DM. 2000. *J. Chem. Phys.* 112:8847–54
194. de Boeij WP, Pshenichnikov MS, Wiersma DA. 1998. *Annu. Rev. Phys. Chem.* 49:99–123
195. Cina JA. 2000. *J. Chem. Phys.* 113:9488–96
196. Hybl JD, Albrecht AW, Faeder SMG, Jonas DM. 1998. *Chem. Phys. Lett.* 297:307–313
197. Keusters D, Tan HS, Warren WS. 1999. *J. Phys. Chem.* 103:10369–80
198. Hahn EL. 1950. *Phys. Rev.* 80:580–94
199. Ernst RR, Bodenhausen G, Wokaun A. 1987. *Principles of Nuclear Magnetic Resonance in One and Two Dimensions.* New York: Oxford Univ. Press
200. Kurnit NA, Abella ID, Hartmann SR. 1964. *Phys. Rev. Lett.* 13:567–70
201. Patel CKN, Slusher RE. 1968. *Phys. Rev. Lett.* 20:1087–89
202. Fleming GR, Cho MH. 1996. *Annu. Rev. Phys. Chem.* 47:109–34
203. Pastirk I, Lozovoy VV, Dantus M. 2001. *Chem. Phys. Lett.* In press
204. Lozovoy VV, Grimberg BI, Pastirk I, Dantus M. 2001. *Chem. Phys. (Special issue Laser Control of Quantum Dynamics).* In press
205. Schmitt M, Knopp G, Materny A, Kiefer W. 1997. *Chem. Phys. Lett.* 280:339–47
206. Schmitt M, Knopp G, Materny A, Kiefer W. 1997. *Chem. Phys. Lett.* 270:9–15
207. Meyer S, Schmitt M, Materny A, Kiefer W, Engel V. 1997. *Chem. Phys. Lett.* 281:332–36
208. Meyer S, Schmitt M, Materny A, Kiefer W, Engel V. 1998. *Chem. Phys. Lett.* 287:753–54
209. Siebert T, Schmitt M, Michelis T, Materny A, Kiefer W. 1999. *J. Raman Spectrosc.* 30:807–13
210. Fayer MD. 1982. *Annu. Rev. Phys. Chem.* 33:63–87
211. Rose TS, Wilson WL, Wäckerle G, Fayer MD. 1987. *J. Chem. Phys.* 86:5370–91
212. Dhar L, Rogers JA, Nelson KA. 1994. *Chem. Rev.* 94:157–93
213. Morgen M, Price W, Ludowise P, Chen Y. 1995. *J. Chem. Phys.* 102:8780–89

214. Lavorel B, Faucher O, Morgen M, Chauv R. 2000. *J. Raman Spectrosc.* 31:77–83
215. Frey HM, Beaud P, Gerber T, Mischler B, Radi PP, Tzannis AP. 2000. *J. Raman Spectrosc.* 31:71–76
216. Brown EJ, Zhang Q, Dantus M. 1999. *J. Phys. Chem.* 110:5772–88
217. Morgen M, Price W, Hunziker L, Ludowise P, Blackwell M, Chen Y. 1993. *Chem. Phys. Lett.* 209:1–9
218. Heritage JP, Gustafson TK, Lin CH. 1975. *Phys. Rev. Lett.* 34:1299–1302
219. Felker PM, Baskin JS, Zewail AH. 1986. *J. Chem. Phys.* 90:724–28
220. Baskin JS, Fekler PM, Zewail AH. 1986. *J. Chem. Phys.* 84:4708–10
221. Dantus M, Bowman RM, Baskin JS, Zewail AH. 1989. *Chem. Phys. Lett.* 159:406–12
222. Baskin JS, Zewail AH. 1994. *J. Phys. Chem.* 98:3337–51
223. Connell LL, Corcoran TC, Joireman PW, Felker PM. 1990. *J. Phys. Chem.* 94:1229–32
224. Felker PM. 1992. *J. Phys. Chem.* 96:7844–57
225. Hayden CC, Chandler DW. 1995. *J. Chem. Phys.* 103:10465–72
226. Herzberg G. 1966. *Molecular Spectra and Molecular Structure. III. Electronic Spectra and Electronic Structure of Polyatomic Molecules.* New York: van Nostrand
227. Herzberg G. 1991. *Molecular Spectra and Molecular Structure. I. Diatomic Molecules.* New York: van Nostrand
228. Clark RJH, Rippon DM. 1973. *J. Chem. Soc. Faraday Trans. 2.* 69:1496–1501
229. Cho M, Du M, Scherer NF, Fleming GR. 1993. *J. Chem. Phys.* 99:2410–28
230. Spiridonov VP, Gershikov AG, Butayev BS. 1979. *J. Mol. Struct.* 52:53–62
231. Friedrich B, Herschbach D. 1995. *Phys. Rev. Lett.* 74:4623–26
232. Kim W, Felker PM. 1996. *J. Chem. Phys.* 104:1147–50
233. Dion CM, Keller A, Atabek O, Bandrauk AD. 1999. *Phys. Rev. A* 59:1382–91
234. Villeneuve DM, Aseyev SA, Dietrich P, Spanner M, Ivanov MY, Corkum PB. 2000. *Phys. Rev. Lett.* 85:545–42
235. Lopez-Martens RB, Schmidt TW, Roberts G. 2000. *Phys. Rev. A* 62:13414–19
236. Lewenstein M, Balcoup P, Ivanov MY, Lhuillier A, Corkum PB. 1994. *Phys. Rev. A* 49:2117–32
237. Dietrich P, Burnett NH, Ivanov M, Corkum PB. 1994. *Phys. Rev. A* 50:R3585–88
238. Zuo T, Bandrauk AD. 1995. *J. Nonlinear Opt. Phys. Mater.* 4:533–46
239. Constant E, Taranukhin VD, Stolow A, Corkum PB. 1997. *Phys. Rev. A* 56:3870–78
240. Sheehy B, Martin JDD, DiMauro LF, Agostini P, Schafer KJ, et al. 1999. *Phys. Rev. Lett.* 83:5270–73
241. Bandrauk AD, Yu HT. 1999. *Phys. Rev. A* 59:539–48
242. Bartels R, Backus S, Zeek E, Misoguti L, Vdovin G, et al. 2000. *Nature* 406:164–66
243. Schumacher DW, Bucksbaum PH. 1996. *Phys. Rev. A* 54:4271–78
244. Hertlein MP, Bucksbaum PH, Muller HG. 1997. *J. Phys. B* 30:L197–205
245. Bensity TJ, Haefliger G, Jones RR. 1997. *Phys. Rev. Lett.* 79:2018–21
246. van Leeuwen R, Bajema ML, Jones RR. 2000. *Phys. Rev. A* 6102:2716–17
247. Villeneuve DM, Ivanov MY, Corkum PB. 1996. *Phys. Rev. A* 54:736–41
248. Yoneda H, Hasegawa N, Kawana S, Ueda K. 1999. *Fusion Eng. Design* 44:141–46
249. Riley D, Woolsey NC, McSherry D, Weaver I, Djaoui A, Nardi E. 2000. *Phys. Rev. Lett.* 84:1704–7
250. Pauling L. 1955. *Angew. Chem.* 67:241–60
251. Polanyi JC. 1987. *Angew. Chem. Int. Ed. Engl.* 26:952–71
252. Zewail AH. 2000. *J. Phys. Chem. A* 104:5660–94



253. Hoganson CW, Babcock GT. 1997. *Science* 277:1453–56
254. Tommos C, Babcock GT. 1998. *Acc. Chem. Res.* 31:18–25
255. Schelvis JPM, Varotsis C, Deinum G, Babcock GT. 1999. *Laser Chem.* 19:223–25
256. Okunishi M, Hashimoto J, Chiba H, Ohmori K, Ueda K, Sato Y. 1999. *J. Phys. Chem. A* 103:1734–41
257. Ohmori K, Kurosawa T, Chiba H, Okunishi M, Sato Y, et al. 1999. *Chem. Phys. Lett.* 315:411–15
258. Tanimura Y, Mukamel S. 1993. *J. Chem. Phys.* 99:9496–511
259. Ivanecky JE, Wright JC. 1993. *Chem. Phys. Lett.* 206:437
260. Tominaga K, Keogh GP, Naitoh Y, Yoshihara K. 1995. *J. Raman Spectrosc.* 26:495–501
261. Steffen T, Duppen K. 1996. *Phys. Rev. Lett.* 76:1224–27
262. Tominaga K, Yoshihara K. 1996. *Phys. Rev. Lett.* 76:987–90
263. Tominaga K, Yoshihara K. 1996. *J. Chem. Phys.* 104:4419–26
264. Tominaga K, Yoshihara K. 1997. *Phys. Rev. A* 55:831–34
265. Tokmakoff A, Lang MJ, Larsen DS, Fleming GR. 1997. *Chem. Phys. Lett.* 272:48–54
266. Tokmakoff A, Fleming GR. 1997. *J. Chem. Phys.* 106:2569–82
267. Steffen T, Duppen K. 1997. *Chem. Phys. Lett.* 273:47–54
268. Ulness DJ, Kirkwood JC, Albrecht AC. 1998. *J. Chem. Phys.* 108:3897–902
269. Blank DA, Kaufman LJ, Fleming GR. 1999. *J. Chem. Phys.* 111:3105–14
270. Kirkwood JC, Albrecht AC. 2000. *J. Raman Spectrosc.* 31:107–24
271. Astinov V, Kubarych KJ, Milne CJ, Miller RJD. 2000. *Chem. Phys. Lett.* 327:334–42
272. Astinov V, Kubarych KJ, Milne CJ, Miller RJD. 2000. *Opt. Lett.* 25:853–55
273. Lozovoy VV, Pastirk I, Comstock M, Dantus M. 2001. *Chem. Phys.* In press
274. Yan ZC, Seideman T. 1999. *J. Chem. Phys.* 111:4113–20
275. Seideman T. 1999. *J. Chem. Phys.* 111:4397–405

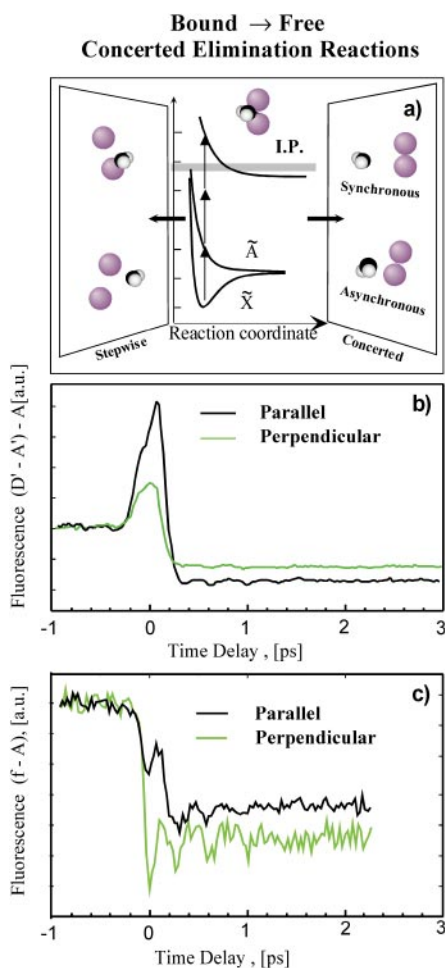


**Figure 2** (a) Potential energy surfaces for  $\text{CH}_2\text{I}_2$  in the gas phase showing stepwise (left) and concerted (right) photodissociation pathways following excitation by the pump pulse (312 nm). The concerted mechanisms are responsible for the production of  $\text{I}_2$  in the  $D'$  and  $f$  excited states as well as carbene. The concerted synchronous mechanism involves the simultaneous breakage of two C-I bonds and the formation of the I-I bond, while the concerted asynchronous mechanism requires the asymmetric progress of the reaction such that one C-I bond starts breaking before the other, but all bond rearrangement takes place in a single kinetic step. The later mechanism results in large rotational excitation of the product. (b) Transients obtained by depletion probing of the  $D' \rightarrow A'$  fluorescence collected at 340 nm of the nascent  $\text{I}_2(D')$  product, for pulses polarized parallel (black) and perpendicular (green) to each other. (c) Transients obtained by depletion probing of the  $f \rightarrow A$  fluorescence collected at 272 nm of the nascent  $\text{I}_2(f)$  product, for pulses polarized parallel (black) and perpendicular (green) to each other.

## Free $\rightarrow$ Bound Bimolecular Reactions Femtosecond Photoassociation Spectroscopy

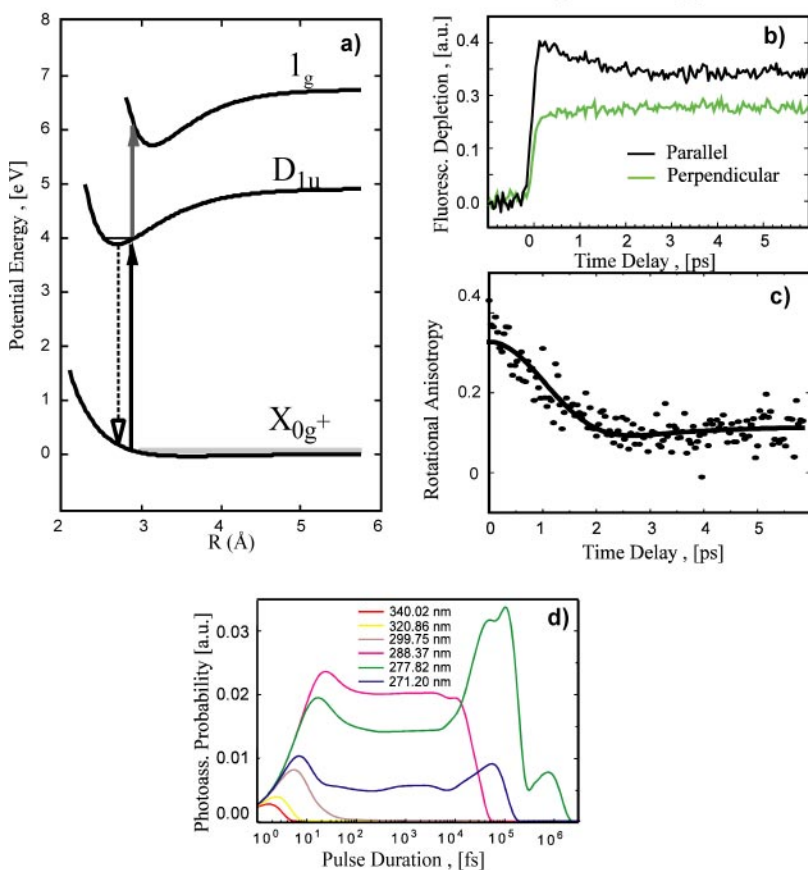


**Figure 4** (a) Potential energy surfaces involved in the photoassociation reaction of Hg atoms.  $Hg_2$  is formed in the  $D1_u$  state after the pump pulse is applied. The probe pulse causes a depletion of the  $D1_u$  state population by exciting the molecules into the  $1_g$  state. (b) Fluorescence signal of  $Hg_2 D1_u \rightarrow X0_g^+$  as a function of the delay between the pump and the probe pulses, for pulses polarized parallel and perpendicular to each other. At time zero, a sudden onset of the fluorescence takes place indicating that the photoassociated molecules are formed within the pulse duration. The maximum depletion probability corresponds to collision pairs that are aligned parallel with respect to the probing pulse. (c) Rotational anisotropy obtained from the experimental data (dots) and from a numerical fitting (line). The rotational dephasing of the initial anisotropy results from the rotational distribution of the excimers respect to a central rotational level. (d) Calculated photoassociation probability assuming a constant initial colliding energy, as a function of pulse duration for different binding pulse wavelengths.

## Spin Echo and Photon Echo Phenomena

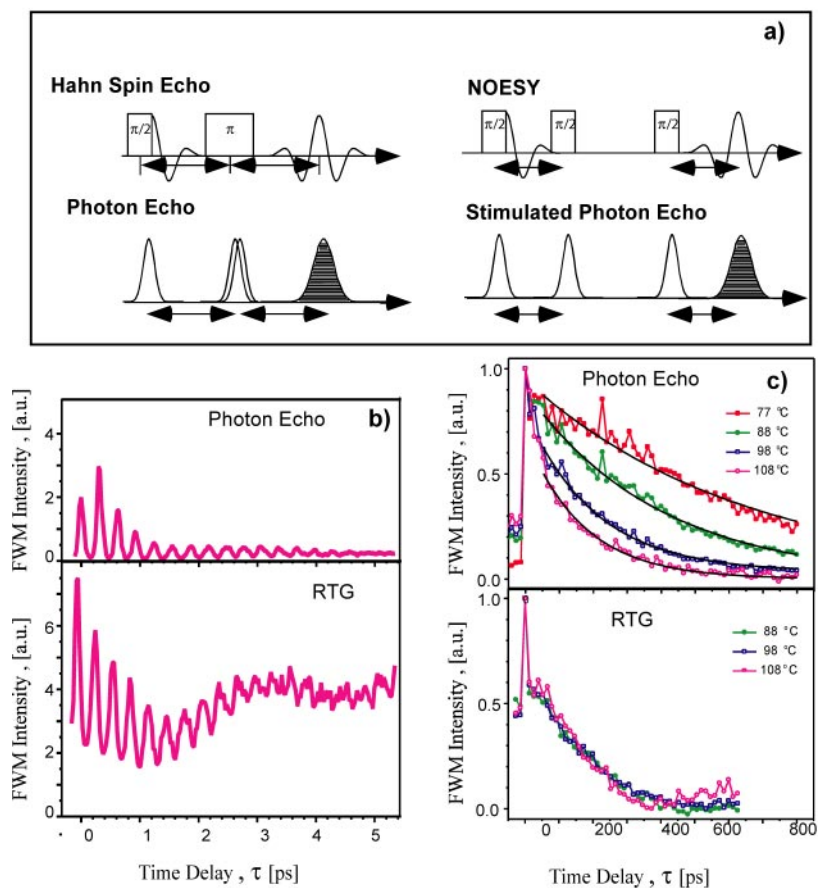
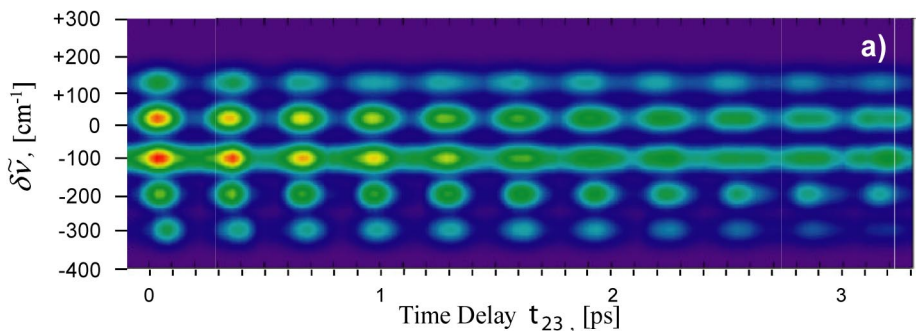


**Figure 7** (a) Schematic representation of the Hahn spin echo and of the Nuclear Overhauser Effect Spectroscopy (NOESY) pulse sequences used in nuclear magnetic resonance (*top*) and their optical counterparts, photon echo (PE) and stimulated photon echo (*bottom*). (b) Experimental time-integrated transients for photon echo and reverse transient grating (RTG) pulse sequences as a function of time delay between the scanned and the overlapped pulses. The PE signal is observed to be background free while the RTG data is strongly modulated by a dephasing process with a dip at 1.4 ps. (c) Homogenous vibronic coherence relaxation measurements of molecular iodine as a function of temperature using the PE (*top*) pulse sequence. When the RTG pulse sequence is used (*bottom*), we observe a temperature independent decay suggesting the large inhomogeneous relaxation process overwhelms the homogeneous rate of relaxation.

## Time-Resolved Frequency-Dispersed FWM The Effect of Linear Chirp

$$t_{12} = 460 \text{ fs}, \text{ chirp} = 0$$



$$t_{12} = 460 \text{ fs}, \text{ chirp} = 3300 \text{ fs}^2$$

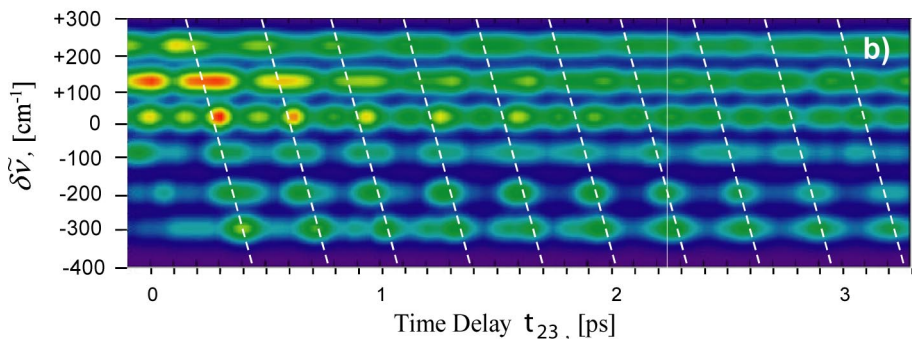


**Figure 9** (a) Experimental time-resolved frequency dispersed FWM data for iodine vapor with  $\tau_{12} = 460$  fs and transform limited pulses. This two dimensional contour plot shows only 307 fs oscillations from the excited state dynamics. There is no evidence of ground state dynamics contribution and all spectral components oscillate in phase. (b) Experimental time-resolved frequency dispersed data when  $\tau_{12} = 460$  fs and  $\phi'' = 3300 \text{ fs}^2$ . The chirped pulses lead to the formation of a chirped vibrational wave packet in the excited state. The dotted lines correspond to the chirp magnitude of the lasers. Note that the signal on the anti-Stokes side  $\delta\tilde{\nu} > 0$  contains some contribution from ground and excited state dynamics.

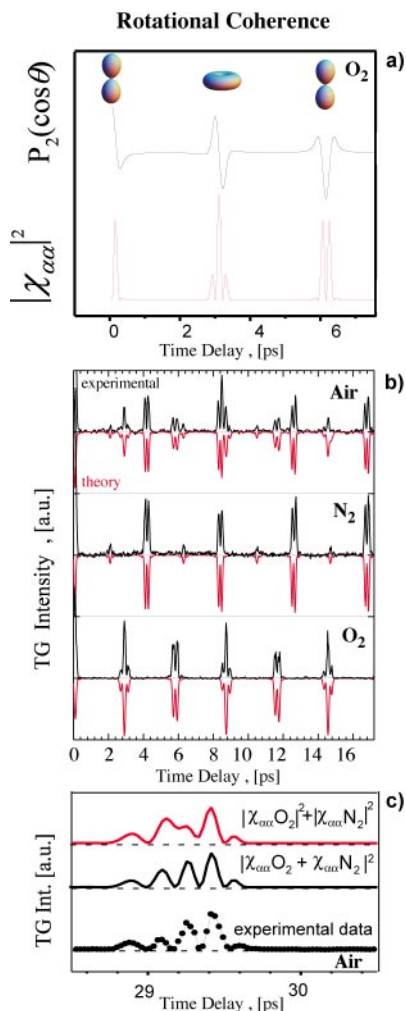


**Figure 10** (a) Simulation of the time-dependent alignment  $P_2(\cos\theta(\tau))$ , and the impulsive coherent Raman scattering signal, proportional to  $|\chi_{\alpha\alpha}(\tau)|^2$ , for  $O_2$ . (b) Experimental (black) and theoretical (red) transient grating (TG) transients of air, nitrogen, and oxygen. Full rotational recurrences are observed at 4.15 ps for  $N_2$  and at 5.77 ps for  $O_2$ . Half recurrences are also observed. The peaks in the air transient directly correspond to recurrences in the  $N_2$  and  $O_2$  scans. Simulated TG signals for these samples were calculated using Equation (9). Note that in the simulations, the full and half recurrences are reproduced at the same recurrence times and with the same intensity and shape as in the experimental signal. (c) Experimental TG signal from air for time delay in the range of 29 to 30 ps (dots). Simulations of the data using two models, the sum of  $O_2$  and  $N_2$  signals (red) and of the square of the sum of the  $O_2$  and  $N_2$  susceptibilities (black). The later simulation gives the best fit of the experimental data.

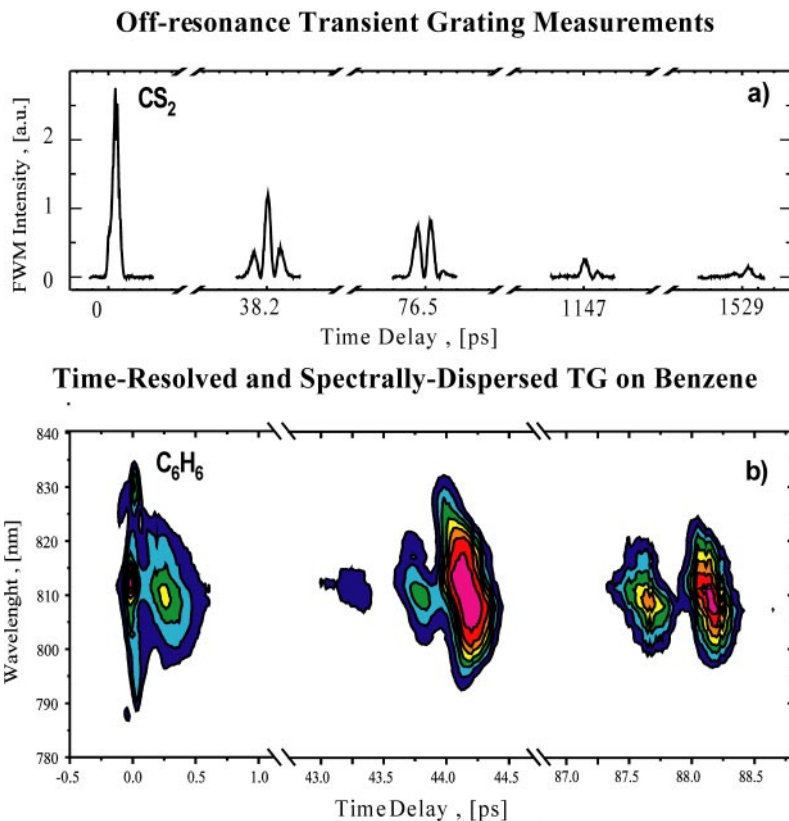


**Figure 11** (a) Off-resonance transient grating experimental data obtained from carbon disulfide vapor. Half rotational recurrences are observed at 38.2 and 114.7 ps while full rotational recurrences are observed at 76.5 and 152.9 ps. (b) Off-resonance transient grating experimental data obtained from benzene vapor. The time-resolved spectrally dispersed signal is detected with a spectrometer and CCD detector. The initial feature corresponds to time-zero observed because of the instantaneous polarizability of the sample. The feature near 2.5 ps is caused by the initial rotational dephasing. The subsequent features correspond to the first and second rotational recurrences. Notice that the time axis is not continuous.



## CONTENTS

A Free Radical, <i>Alan Carrington</i>	1
State-to-State Chemical Reaction Dynamics in Polyatomic Systems: Case Studies, <i>James J Valentini</i>	15
Recent Progress in Infrared Absorption Techniques for Elementary Gas-Phase Reaction Kinetics, <i>Craig A Taatjes, John F Hershberger</i>	41
Surface Biology of DNA by Atomic Force Microscopy, <i>Helen G Hansma</i>	71
On the Characteristics of Migration of Oligomeric DNA in Polyacrylamide Gels and in Free Solution, <i>Udayan Mohanty, Larry McLaughlin</i>	93
Mechanisms and Kinetics of Self-Assembled Monolayer Formation, <i>Daniel K Schwartz</i>	107
Crossed-Beam Studies of Neutral Reactions: State-Specific Differential Cross Sections, <i>Kopin Liu</i>	139
Coincidence Spectroscopy, <i>Robert E Continetti</i>	165
Spectroscopy and Hot Electron Relaxation Dynamics in Semiconductor Quantum Wells and Quantum Dots, <i>Arthur J Nozik</i>	193
Ratiometric Single-Molecule Studies of Freely Diffusing Biomolecules, <i>Ashok A Deniz, Ted A Laurence, Maxime Dahan, Daniel S Chemla, Peter G Schultz, Shimon Weiss</i>	233
Time-Resolved Photoelectron Spectroscopy of Molecules and Clusters, <i>Daniel M Neumark</i>	255
Pulsed EPR Spectroscopy: Biological Applications, <i>Thomas Prisner, Martin Rohrer, Fraser MacMillan</i>	279
Fast Protein Dynamics Probed with Infrared Vibrational Echo Experiments, <i>Michael D Fayer</i>	315
Structure and Bonding of Molecules at Aqueous Surfaces, <i>GL Richmond</i>	357
Light Emitting Electrochemical Processes, <i>Neal R Armstrong, R Mark Wightman, Erin M Gross</i>	391
Reactions and Thermochemistry of Small Transition Metal Cluster Ions, <i>PB Armentrout</i>	423
Spin-1/2 and Beyond: A Perspective in Solid State NMR Spectroscopy, <i>Lucio Frydman</i>	463
From Folding Theories to Folding Proteins: A Review and Assessment of Simulation Studies of Protein Folding and Unfolding, <i>Joan-Emma Shea, Charles L Brooks III</i>	499
Polymer Adsorption-Driven Self-Assembly of Nanostructures, <i>Arup K Chakraborty, Aaron J Golubfskie</i>	537
Biomolecular Solid State NMR: Advances in Structural Methodology and Applications to Peptide and Protein Fibrils, <i>Robert Tycko</i>	575
Photofragment Translational Spectroscopy of Weakly Bound Complexes: Probing the Interfragment Correlated Final State Distributions, <i>L Oudejans, RE Miller</i>	607
Coherent Nonlinear Spectroscopy: From Femtosecond Dynamics to Control, <i>Marcos Dantus</i>	639
Electron Transmission through Molecules and Molecular Interfaces, <i>Abraham Nitzan</i>	681



Early Events in RNA Folding, <i>D Thirumalai, Namkyung Lee, Sarah A Woodson, DK Klimov</i>	751
Laser-Induced Population Transfer by Adiabatic Passage Techniques, <i>Nikolay V Vitanov, Thomas Halfmann, Bruce W Shore, Klaas Bergmann</i>	763
The Dynamics of "Stretched Molecules": Experimental Studies of Highly Vibrationally Excited Molecules with Stimulated Emission Pumping, <i>Michelle Silva, Rienk Jongma, Robert W Field, Alec M Wodtke</i>	811